Comparison of methods to derive the height-area relationship of shallow lakes in West Africa using remote sensing

F. Girard [1,2], L. Kergoat [1], H. Nikiema[3], M. Wubda[4], R. Yonaba[5], T. Fowé[5], A. Abdourhamane Touré[6], I. Mainassara[7,8], M. de Fleury[1]and M. Grippa [1]

[1]Géosciences Environnement Toulouse (GET, Université de Toulouse, CNRS, IRD, CNES), Toulouse, France.

[2]Collecte Localisation Satellites (CLS), Ramonville-Saint-Agne, France.

[3]LERMIT, Université Joseph Ki-Zerbo, Ouagadougou, Burkina Faso.

[4]Université Joseph Ki-Zerbo, UFR-SVT/DST, Ouagadougou, Burkina Faso.

[5]Laboratoire Eaux, Hydro-Systèmes et Agriculture (LEHSA), Institut International d'Ingénierie de l'Eau et de l'Environnement (2iE), Ouagadougou, Burkina Faso.

[6]Université Abdou Moumouni, Faculté des Sciences et Techniques, Département de Géologie, Niamey, Niger.

[7]HydroSciences Montpellier (HSM, Univ Montpellier, CNRS, IRD) Montpellier, France.

[8]Représentation IRD au Niger, Niamey, Niger

Key Points:

- Four different remote sensing methods to derive volume changes of small and medium-sized shallow lakes have been intercompared.
- All methods, based on radar and lidar altimetry, Sentinel-2 water areas, and Pleiades Digital Surface Models, show good performances.
- Pros and cons of each method are identified and discussed.

Corresponding author: Félix Girard, `felix.girard@get.omp.eu`

Abstract

In West Africa, lakes and reservoirs play a vital role as they are critical resources for drinking water, livestock, irrigation and fisheries. Given the scarcity of in-situ data, satellite remote sensing is an important tool for monitoring lake volume changes in this region. Several methods have been developed to do this using water height and area relationships, but few publications have compared their performance over small and medium-sized lakes. In this work we compare four methods based on recent data from the Pleiades, Sentinel-2 and -3, ICESat-2 and GEDI missions over 16 lakes in the Central Sahel, ranging in area from 0.22 km^2 to 21 km^2. All methods show consistent results and are generally in good agreement with in-situ data (height RMSE and volume NRMSE mostly below 0.30m and 11% respectively). The obtained height-area relationships show very little noise (fit RMSD mostly below 0.10m), except for the Sentinel-3-based method which tends to produce higher dispersion. The precision of the estimated water height is about 0.20m for Pleiades Digital Surface Models (DSMs) and less than 0.13m for the other methods. In addition, fine shape patterns are consistently observed over small height amplitudes, highlighting the ability to monitor shallow lakes with non-linear bathymetric behavior. Inherent limitations such as DSM quality, temporal coverage of DSM and lidar data, and spatial coverage of radar altimetry data are identified. Finally, we show that the combination of lidar and radar altimetry-based methods has great potential for estimating water volume changes in this region.

1 Introduction

Lakes store 87% of surface liquid freshwater on Earth (Gleick, 1993). Even though the main freshwater stocks are located in glaciers and underground (Oki & Kanae, 2006), lakes are a crucial component of the water cycle as they provide a readily accessible water resource. Their number is dominated by abundant small water bodies and ponds (Biggs et al., 2017) whereas medium-sized and large lakes (size $>$ 1km^2) represent 85% of the global lake area (Pi et al., 2022). Lakes and reservoirs provide crucial services for humans (Reynaud & Lanzanova, 2017) and ecosystems (Schallenberg et al., 2013) such as freshwater and food supply, electricity, nutrients processing, natural habitats and recreational services. The capability of lakes to ensure these services inherently depends on their water storage.

Monitoring lake volume change is essential as several recent studies highlighted significant variations over the past decades. For instance, Wurtsbaugh et al. (2017) demonstrated that many of the world's saline lakes are shrinking at an important rate. Yao et al. (2023) identified a decline of lake water volume over 53% of the 1972 largest global lakes, with the majority of the loss attributable to direct human activities and climate change. Even though lake desiccation trends are widespread, the Yao et al. study, consistently with Luo et al. (2022) and (Wang et al., 2018), also revealed regional patterns with net water volume gains in areas such as the Inner Tibetan Plateau and the Northern Great Plains of North America.

The hydrological functioning of water bodies in West Africa is poorly known at the large scale (Papa et al., 2023). Yet areas such as Central Sahel host a multitude of water bodies, ranging from reservoirs (Cecchi et al., 2009), small lakes and ponds (Gardelle et al., 2010; Grippa et al., 2019) and temporary water bodies (Haas et al., 2009), which are widespread but still relatively unknown in number. Being used for drinking water, livestock watering, irrigation and fishing, these water bodies play a vital role in such an area subject to a long dry season (Cecchi et al., 2009; Frenken, 2005). Despite the severe drought that impacted Central Sahel in the 1970s and 1980s, several studies have highlighted a paradoxical increase in the surface area of lakes and ponds (Baba et al., 2019; Gal et al., 2016; Gardelle et al., 2010), as well as an increase in runoff and river discharges (Descroix et al., 2018; Favreau et al., 2009; Mahe et al., 2010). Attempts to study the evolution of water volumes in West Africa have been carried out either at the scale of a few lakes (Fowe et al., 2015; Gal et al.,

2016; Pham-Duc et al., 2020), or at a larger scale but punctually in time (Annor et al., 2009; Cecchi et al., 2009; Liebe et al., 2005). In addition, West African lakes and reservoirs have been included in global studies, but these are brief in time (Cooley et al., 2021) or cover only a few large lakes (Luo et al., 2022; Yao et al., 2023). In this regard, efforts remain to be done for both long-term and large-scale monitoring of the lake volume changes in this region.

Historically, in-situ sensors are used to measure the evolution of lake water level and volume. However, the limited spatial coverage and the global decline of in-situ operations and installations (Papa et al., 2023; Riggs et al., 2023; Schwatke et al., 2015) challenge the capability to have long and large-scale time series. With periodic observations and a considerably increased spatial coverage, satellites are a relevant tool for assessing lake water volume trends globally.

Remote sensing allows measuring physical parameters of water bodies such as water surface height and area. Water surface height is derived from the return time estimation of electromagnetic waves emitted by nadir-looking radar or laser altimeters. Synthetic Aperture Radar (SAR) altimeters such as those on board Sentinel-3 and Sentinel-6 are able to measure the elevation of water bodies of a few hectares with a sub-monthly revisit time (Normandin et al., 2018; Taburet et al., 2020). However, these measurements still suffer from coarse across-track resolutions which may lead to contamination by bright surfaces located in the radar footprint (Boy et al., 2022). In addition, the nadir-viewing and the inter-track distance of several tens of kilometers of the conventional radar altimeters restrict their spatial coverage. The Ice, Cloud and land Elevation Satellite-2 (ICESat-2) and the Global Dynamics Ecosystem Investigation (GEDI) missions carry on board multi-beams laser altimeters enabling along-track surface elevation posting rate from tens of centimeters to tens of meters (Neuenschwander et al., 2023), (Dubayah et al., 2020). Nonetheless, these measurements remain discrete and their temporal coverage is limited by the multi-month revisit time of the satellites and some degraded acquisition periods for GEDI (Urbazaev et al., 2022).

The estimation of the water extent from optical or radar imagery observations is based on the separation of the spectral or backscattering signature of water from that of the soil (Pekel et al., 2016; Yao et al., 2019). With a revisit time of 5 days and a spatial resolution of up to 10m, the Sentinel-2 optical sensors can be used to monitor water surface area variations of a large number of lakes and reservoirs (Reis et al., 2021; Schwatke et al., 2019; Yang et al., 2017). Cloud cover, which is usually one of the main obstacles to optical observation of water bodies, is not a major problem in West Africa since the dry season lasts between 6 and 9 months (Nicholson, 2018).

Water surface height and area can be combined to calculate volume changes between consecutive observations. This is usually done by assuming that the observed portion of the lake behaves like a cone or pyramid frustum (Crétaux et al., 2016; Luo et al., 2022; Terekhov et al., 2020), or by multiplying the water level change by the average surface area between the two dates (Gao et al., 2012; Li et al., 2020; Song et al., 2013). These two solutions require simultaneous observations of water surface height and area and are based on geometric approximations whose accuracy decreases as the water level change increases. A third way consists of using the height-area relationship (Abileah et al., 2011), which synthesizes the lake's bathymetry information into a relationship that describes changes in surface area as a function of water level. Once the height-area relationship has been constructed, volume change can be calculated by integration (Carabajal & Boy, 2021; Duan & Bastiaanssen, 2013; Magome et al., 2003) and using only one of the two variables.

The construction of the height-area relationship requires computing the height and extent of the lake banks contour lines (isobaths). With remote sensing data, isobaths are typically calculated by combining near-simultaneous (within a few days) observations of water surface height and area from radar or lidar altimetry data and imagery respectively

(Abileah et al., 2011; Busker et al., 2019; Gao et al., 2012; Schwatke et al., 2020). Bank topography data such as global Digital Elevation Models (DEM) generated before impoundment or at low water levels have been combined with satellite images to retrieve the water surface elevation of lakes that cannot be observed by altimeters (Avisse et al., 2017; Bhagwat et al., 2019; Terekhov et al., 2020; Tseng et al., 2016). In addition, height-area relationships can also be generated through the analysis of a DEM alone. This method enabled studying the volume changes of many medium-sized and large lakes worldwide (Fang et al., 2019; Pan et al., 2013; Yao et al., 2018; S. Zhang & Gao, 2020). Publications such as Arsen et al. (2013); Bacalhau et al. (2022); Ma et al. (2019); N. Xu et al. (2020) have taken advantage of the high spatial resolution and vertical accuracy of lidar altimetry data to determine not the elevation of the water surface but that of the banks. Unlike DEMs, this bank topography data is discrete but, once intersected with water contours derived by satellite imagery, has shown great potential for bathymetry retrieval above the lowest observed water level.

In terms of intercomparison of methods, Magome et al. (2003) estimated volume change of Lake Volta in Ghana by comparing different methods using altimetry (TOPEX/Poseidon) and optical imagery (Moderate-Resolution Imaging Spectroradiometer, MODIS) or their combination with a DEM. They obtained better results when combining altimetry and DEM and highlighted the greater spatial coverage of the method using the combination of imagery and DEM. Zolá and Bengtsson (2007) also compared several methods over lake Poopó in Bolivia using echo-sounding measurements, combination of Landsat-5 with in situ water heights, and water balance calculations. They found consistent results and good complementarity between the different methods. Apart from these publications, both focusing on large lakes ($> 100\text{km}^2$), few studies have attempted to intercompare different methods to provide height-area relationships, on smaller lakes and with recent data. The aim of this work is to intercompare four different methods based on recent data (Pleiades, Sentinel-2, Sentinel-3, ICESat-2, GEDI) over 16 small ($< 1\text{km}^2$) and medium-sized (1-100km^2) lakes located in Central Sahel. The results of each method are evaluated using criteria of accuracy, precision, sensitivity to surface characteristics and spatio-temporal coverage. The study area, data and methods are described in Section 2 and the comparison results are presented in Section 3 and further discussed in Section 4.

2 Material and methods

2.1 Study area and in-situ data

The study area is mainly located in Central Sahel, between the 10.8°N and 15.5°N latitudes and extends over Mali, Niger and Burkina Faso (BF). From North to South, the climate is semi-arid and dry sub-humid. Rainfall is driven by a tropical monsoon system and follows a latitudinal gradient with mean annual precipitation ranging, from the North to the South, from 200mm.yr^{-1} to 1000mm.yr^{-1}. Rainfall is concentrated during the wet season stretching from June to October. The rest of the year gives way to a long dry season with a very little cloud cover, which is suited for observing water bodies using optical imagery.

Sixteen lakes have been selected according to the in-situ and remote sensing data availability or to existing knowledge and documentation (Figure 1 and Table S1). They are spread along the climatic gradient and include three lakes in Mali, two in Niger and eleven in Burkina Faso.

Ten of these water bodies are reservoirs and others are natural lakes. Their mean altitude varies between 200 and 500m above mean sea level, their mean water surface area ranges from 0.22km^2 (Bangou Kirey) to 21km^2 (Kokorou), and most of them are relatively shallow (a few meters deep). These lakes show different optical water types with varied levels of turbidity, from moderately turbid (Robert et al 2016) to very turbid (e.g. lake Bangou Kirey, (Touré et al., 2016), and some of them harbor temporary or permanent aquatic vegetation (Gardelle et al., 2010; Baba et al., 2019).

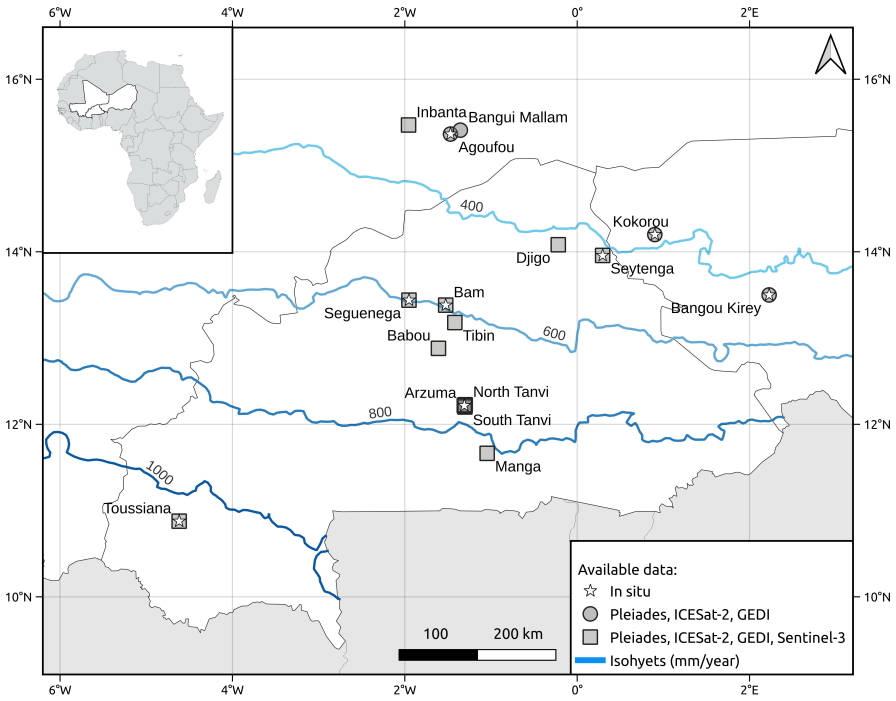

Figure 1. Study area and lakes analyzed in this study.

in-situ data are of different nature and come from different sources. Water surface height data are measured continuously, every 30 minutes, through pressure transducers on the Bangou Kirey lake and the Arzuma reservoir, respectively since July 2022 and March 2023. Additional water surface height measurements have been collected on the Agoufou lake by AMMA-CATCH observatory (Galle et al., 2018) between 2015 and 2019 with a weekly or monthly frequency. Height-volume (H-V) relationships of the Burkinabe reservoirs of Bam, Seguenega and Seytenga have been provided by the Direction Générale des Ressources en Eau (DGRE) in Burkina Faso and come from topographic survey performed before the dams impoundment. Finally, the height-area (H-A) and height-volume-area (H-V-A) relationships of the Kokorou lake and the Toussiana reservoir are extracted respectively from the digitization of Baba et al. (2019) and from Sanogo and Dezetter (1997).

2.2 Satellite data, water surface area and height extraction

2.2.1 Water surface areas and contours from Sentinel-2 optical images

Sentinel-2A and -2B acquire high-resolution multispectral images with a revisit time of approximately 5 days (Table 1). The MultiSpectral Instrument (MSI) onboard Sentinel-2 has 13 spectral bands from blue to Short-Wave InfraRed (SWIR), with spatial resolution from 10m to 60m on the ground. For this study, we use the green and SWIR bands which have resolutions of 10m and 20m. Images are L2A Surface Reflectance (SR) products corrected from atmospheric effects with Sen2Corr processing. Images are downloaded through Google Earth Engine (GEE, (Gorelick et al., 2017)) as the "COPERNICUS/S2_SR" collection, over December 2018 to December 2022. All bands are downscaled to a pixel size of 20m x 20m and images with a percentage of cloudy pixels greater than 5% are discarded. The residual cloudy pixels are masked using the QA cloud and cirrus bitmasks, and an empirical threshold of 0.2 on the blue reflectance. After these steps, a few remaining images (usually

less than 5 per lake) contaminated by clouds or aerosols have been discarded after visual inspection.

To compute water surface area, we mask water pixels by applying a threshold on the MNDWI (H. Xu, 2006), which is a spectral index commonly used to detect water on optical images, based on the normalized difference between the green (B3) and the short-wave infrared (B12) bands.

$$MNDWI = \frac{green - SWIR}{green + SWIR}$$

First, we clip the images to the close surroundings of the water body to exclude close but unconnected water bodies. Then, the MNDWI is computed and the threshold, constant in time, is determined ad hoc for each lake following De Fleury et al. (2023) and Reis et al. (2021). Reis et al. (2021) have shown that water detection is usually accurate for a full range of MNDWI thresholds rather than a well-defined value. The water surface area is finally calculated by counting the number of pixels above the threshold and multiplying by the pixel area. The water contour is delineated using the marching squares algorithm, a 2D adaptation of the marching cubes algorithm (Lorensen & Cline, 1987) which is implemented in the "find contours" function from the Scikit-image Python package. This function takes as input the MNDWI pixels raster and the threshold value and generates iso-value contours at a sub-pixel scale by linearly interpolating the MNDWI pixel values. If the lake separates into several parts as it dries up, we keep only the largest part. For each lake, a time series of water surface areas and water contours is eventually generated.

2.2.2 Pleiades Digital Surface Model

Pleiades-1A and -1B Pleiades are two satellites equipped with a very high-resolution optical sensor acquiring panchromatic images (480-830nm) with a pixel size of 0.50m (Table 1 and Figure 3). We ordered the acquisition of pairs of cloud-free Pleiades panchromatic stereo-images (Pleiades ©CNES 2021, 2022, 2023, Distribution Airbus DS) over each lake, with a B/H ratio between 0.35 and 0.8. Pleiades images allow the creation of Digital Surface Models (DSM) by photogrammetric processing through the computation of matching pixels displacement between two stereo-images. DSMs were processed using the Digital Surface Model from OPTical stereoscopic very-high resolution imagery (DSM-OPT) online service, based on the MicMac tool (Rupnik et al., 2017) and operated by the Solid Earth ForM@Ter pole of the research infrastructure DATA TERRA. DSM-OPT also provides an ortho-image which is a panchromatic image georeferenced identically to the DSM.

Since DSM estimation by photogrammetry is challenging over the water surface due to low pixel correlation, we ordered Pleiades images at the end of the dry season, when water surface level is minimum, which allows exploring the maximum bank extent. We generated DSMs at 1m x 1m horizontal resolution, in line with Bagnardi et al. (2016). As the semi-arid landscapes of the study area often show small surface roughness (compared to mountainous or forest landscapes for instance), we adapted the correlation window size to 9 x 9 pixels and we used 0.2 as the minimum correlation coefficient for matching (Bagnardi et al., 2016). Due to the large extent of the Bam reservoir, two stereo-pairs acquisitions are needed to observe the northern and southern part of the reservoir. To end up with a single DSM, we generated a DSM for each part and we merged them after applying the Nuth and Kääb method (Nuth & Kääb, 2011) to ensure co-registration. However, a residual elevation bias between the two parts has been observed after co-registration. We corrected it by comparing the DSM of each part with terrain ICESat-2 data and subtracting the respective mean difference.

Some Pleiades DSMs showed along-track undulations which were highlighted when computing the difference with the GLO-30 Copernicus DEM (European Space Agency, 2021). For instance, we observed along-track undulations of several meters in Pleiades-1B-derived DSM of the Bangou Kirey and Kokorou lakes. These undulations have been noticed on many DEMs from several space-borne missions (Hugonnet et al., 2022) and are caused

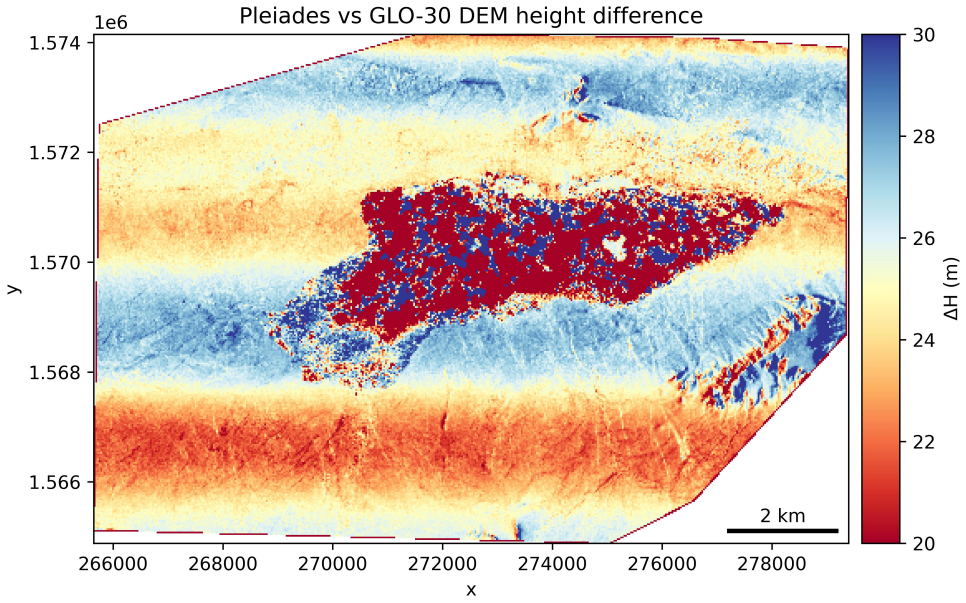

Figure 2. Difference between Pleiades DSM and GLO-30 DEM over Kokorou lake.

by errors in the image geometry estimation due to sensor motion (jitter). Our method to correct for these undulations is partly based on Girod et al. (2017). We compute the average per line of the DEM difference with GLO-30 (Figure 2) and subtract it to the Pleiades DSM.

2.2.3 Bank elevation profile from ICESat-2 lidar altimeter data

The Ice, Cloud and land Elevation Satellite-2 (ICESat-2) was launched in September 2018 (Table 1 and Figure 3) by NASA (Markus et al., 2017). The Advanced Topographic Laser Altimeter System (ATLAS) onboard ICESat-2 is a photon-counting lidar with 3 pairs of laser beams emitting pulses at 10 kHz and separated by 3.3 km in the cross-track direction. The footprint size of each beam has a 14 m diameter. Each pair is composed of a strong beam and a weak beam (energy ratio of 4:1) with a wavelength of 532 nm and located 90 m from each other.

The ATL08 version 6 product is dedicated to land and vegetation and contains along-track heights above the WGS84 ellipsoid for the ground and canopy surfaces (Neuenschwander et al., 2023). We downloaded all ATL08 data over the October 2018 (first data available) - June 2023 period. The nominal posting rate is theoretically 100 m but data gaps can occur due to low signal-to-noise ratio or acquisition errors. For the mid-point of each 100 m segment, ATL08 provides three height metrics, respectively the mean, the median and the best-fit terrain height. The latter is the height resulting from the polynomial which best fits the 100 m terrain profile, among 1st, 3rd and 4th order polynomials. Since the topography of the banks is likely to vary inhomogeneously over 100 m, and as suggested by Tian and Shan (2021), we use the best-fit height in this study. Liu et al. (2021) assessed ICESat-2 ATL08 terrain height data accuracy against airborne lidar products over 40 sites located in the U.S. mainland, Alaska, and Hawaii. They showed that quite similar performances were obtained independently of beam energy, whereas strong beams should theoretically be more accurate because of their better signal-to-noise ratio. They also found nighttime terrain accuracy slightly better than daytime. However, daytime data represent a non-negligible proportion

of the ATL08 data quantity and consequently condition the spatial coverage. Hence, we decided not to filter ATL08 data on the beam energy and acquisition time criteria.

Moreover, the number of terrain photons detected within a segment is important to fit the 100 m height profile and derive a robust estimation of the segment height. Hence, we set a threshold of 10 on the minimum detected number of terrain photons, in line with the results of Urbazaev et al. (2022). To remove large outliers, we keep data with a photon heights STD inferior to 1 m and discard data whose best fit height is inferior to the minimum detected photon height, this being probably due to a fitting error. Finally, given that ICESat-2 beams were purposely mispointing during the first height cycles of the mission, that is during the two first years (nominal cycle of 91 days), certain lakes have irregular or limited temporal coverage.

2.2.4 Bank elevation profile from GEDI lidar altimeter data

The Global Ecosystem Dynamics Investigation mission on board the International Space Station started in December 2018 (Dubayah et al., 2020). It consists of a full-waveform lidar with 3 lasers producing a total of 8 beam ground transects spaced 600 m apart in the cross-track direction. Each ground transect has a footprint size of 30 m and samples the Earth's surface approximately every 60 m along-track (Table 1 and Figure 3). GEDI L2A version 2 data product, distributed by NASA's Land Processes Distributed Active Archive Center (LP DAAC), provides ground elevation, canopy top height and relative height metrics. The ground elevation is represented by the lowest mode elevation which gives the height of the last significant energy return detected in the waveform.

We removed large outliers by rejecting data whose elevation absolute difference with the digital_elevation_model_srtm value, a parameter in the product representing the Shuttle Radar Topography Mission (SRTM) elevation at GEDI footprint location, was greater than 100 m. We also discarded data with a non-zero degrade_flag value, meaning that the lidar shot occurred during a non-degraded period. As for ICESat-2 ATL08 data and following the suggestions of Liu et al. (2021) who assessed GEDI L2A terrain height data accuracy as well, we considered unnecessary to discard GEDI data on the basis of beam energy and acquisition time.

2.2.5 Water surface heights from Sentinel-3 radar altimetry data

The Sentinel-3 (S3) mission includes the Sentinel-3A and 3B satellites carrying on board the Synthetic Aperture Radar Altimeter (SRAL), a delay/Doppler altimeter (Table 1 and Figure 3). The altimeter operates in global mode with an along-track posting rate of approximately 300m and an across-track resolution of several kilometers. Water surface height measurements of the same target are provided every 27 days. Water surface height data have been retrieved from the radar waveforms recorded by Sentinel-3 with the Offset Centre of Gravity (OCOG) retracking algorithm and have been provided by the Centre de Topographie des Océans et de l'Hydrosphère (CTOH). They have been processed using the Altimetric Time Series Software (AlTiS version 2.0, (Frappart et al., 2021)). The data were first selected within a polygon fitted to the lake maximum water extent derived from the corresponding water contour time series. Then, they were filtered with a threshold of 40dB on the backscattering coefficient for data acquired before January 2020, and a threshold of 20dB for data acquired after January 2020 (De Fleury et al., 2023). These thresholds are in line with what is suggested by Taburet et al. (2020) and Kittel et al. (2021). Besides, multi-peak waveforms or dry-lake data were rejected with an empirical threshold of 20 on the waveform peakiness. The resulting water surface height is computed as the median of the remaining height values. Water surface heights with a Median Absolute Deviation (MAD) along the transect greater than 1m are rejected. For each lake, a water surface height time series was eventually generated.

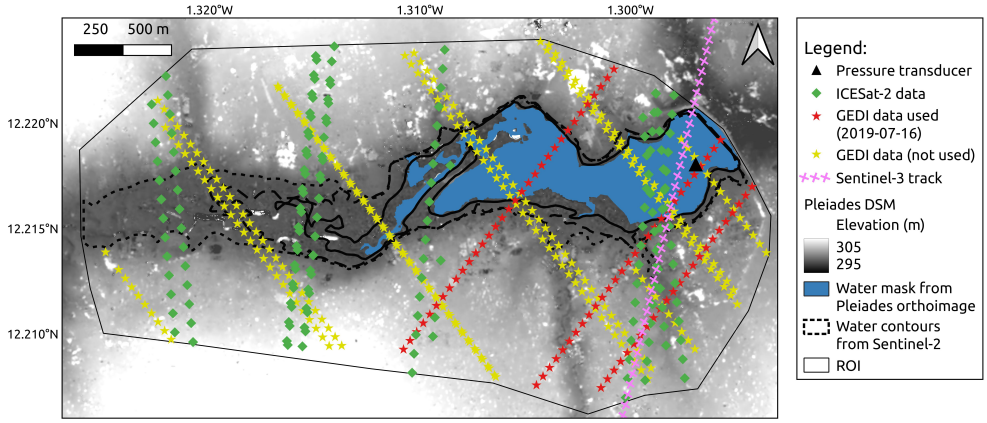

Figure 3. Data available over the Arzuma reservoir. Gray level background is the Pleiades DSM with the corresponding water mask in blue. Pressure transducer is represented by a black triangle. ICESat-2, unused and used GEDI data are respectively represented by green diamonds, yellow and red stars. Sentinel-3 theoretical ground track is represented by magenta crosses. Full, dashed and dotted black lines represent 3 selected water contours computed from Sentinel-2 images.

Table 1. Remote sensing data and corresponding mission used in this study.

Mission	S2	S3	ICESat-2	GEDI	Pleiades
Full name	Sentinel-2	Sentinel-3	Ice, Cloud and Land Elevation Satellite-2	Global Ecosystem Dynamics Investigation	Pleaides
Launch date	Jun 2015 (2A), Mar 2017 (2B)	Feb 2016 (3A), Apr 2018 (3B)	Sep 2018	Dec 2018	Dec 2011 (1A), Dec 2012 (1B)
Product	L2A surface reflectance	L2 OCOG	ATL08 v6	L2A v2	panchromatic stereo
Parameter	water surface area	water surface height	terrain height profile	terrain height profile	2D surface elevation
Revisit time	5 days	27 days	91 days (after Sept. 2020)	variable	
Posting rate	20m x 20m	300m (along-track)	100m (along-track)	60m (along-track)	1m x 1m
Field name	B03, B12	ice1_ku_SurfHeight_alti	h_te_bestfit	elev_lowestmode	

2.3 Methods to derive height-area relationships

2.3.1 DEM filling

This method uses an incremental approach to count DEM pixels whose elevation is between two given altitudes, and repeats the operation over a set of elevation increments until filling the entirety of the banks of the water body. Taking advantage of the DSM Pleiades vertical resolution, the incremental step between two successive elevations of the processing is empirically set to 0.1m. For each elevation increment, the corresponding pixel number is converted to an area by multiplying by the pixel area, and forms an elevation-area pair. All the elevation-area pairs form the H-A curve. Moreover, since the processing stops at an altitude defined manually, it is possible that, at a certain point, the computed water areas exceed the physical reality of the lake dynamics over the study period. The upper limit of the H-A relationship is therefore set to the maximum Sentinel-2-observed water area. For the following, this method will be referred to as the "DSM Pleiades" and is graphically represented in Figure 4a.

A Pleiades DSM footprint is at least 100km^2. We first limit the processed area to the region of interest by clipping the DSM to a polygon representing the close surroundings of the water body. Water surfaces generate "No Data" values or extreme outliers on the DSM due to low pixel correlations during the stereo-matching processing, and have to be filtered out. Hence, we mask water pixels on the orthoimage. Since orthoimage reflectance values generally follow a bi-modal distribution, we separate water from soil by defining a global threshold on the reflectance pixels. Finally, we mitigate the remaining minimal classification errors by filling the holes with a morphological closure using a square structuring element of size 9x9.

Once water has been masked, we determine the altitude of the water surface as the median elevation of the water pixels located along the contour. This contour is computed as the external morphological gradient using a cross structuring element of size 1. In addition, contamination by outliers is mitigated using the MADe method (Kannan et al., 2015).

2.3.2 Intersecting a DEM with water contours

This method is similar to what Mason et al. (1995-12-01) mentions as the "waterline method", and multiple studies such as Ragettli et al. (2021) already employed it to retrieve lake bathymetry. Assuming the water surface is flat, isobaths can be computed as the intersection of water contours with a DEM. The water contours elevation is computed as the median value of the intersected DEM pixels elevations, consecutively to an outliers removal process based on the MADe method. Furthermore, we consider that the water contour must intersect a minimum number of DEM pixels, empirically set as 20. Finally, the lower limit of the H-A relationship is set to the minimum Pleiades-observed water area. For the application of this method on Pleiades DSMs, we will use the term "DSM Pleiades/contours" (Figure 4b).

Since the Pleiades DSM are surface models, they provide elevation of the highest observed point on the ground. Thus, they are impacted by relief like buildings and, particularly for the studied lakes, trees and riparian vegetation. To mitigate this impact, we mask out the obvious wooded parts of the Pleiades DSMs. This is the case for the right banks of the Bangou Kirey lake. The Inbanta lake is densely covered in trees and if all of them were masked the remaining area would be too small to compute the H-A curve. Therefore, for this lake we do not mask out any area. The resulting impact of vegetation will be discussed later.

2.3.3 Intersecting bank elevation profile with water contours

Instead of using a whole DEM providing continuous information of the ground elevation, this method requires one or multiple discrete elevation profiles of the banks of the water body. Here, we use elevation profiles either from ICESat-2 or GEDI lidar topography measurements. This method will be referred to as the "Profile ICESat-2/contours" or "Profile GEDI/contours" method (Figure 4c). As with the DSM-based methods, the water level at the dates the elevation profiles were recorded determines the extent of the bank bathymetry that can be characterized. Isobaths are retrieved by calculating the intersections between the water contours and the banks elevation profile. For this purpose, the profiles are converted to geometric lines and we compute the crossover points with the water contour polygons. The crossover points elevation is linearly interpolated between the two measurement points. It is important to check that the pair of measurement points was acquired over the ground and not over water, and that they are located on the same bank, otherwise the resulting interpolated elevation will be erroneous. To do this, we mask out the measurement points acquired over water using the closest Sentinel-2 image in time.

We empirically set a maximal threshold of 2% on the bank slope to reject crossover points located at places too steep with respect to lidar data posting rate. Then, because it is more robust than the mean, the median value of the crossover points elevations is retained for the water contour elevation, following Arsen et al. (2013). Finally, we filter out water contours whose elevation is computed from only one crossover point, as it may reflect erroneous intersections due to small water contour detection errors. Given the multiplicity of the laser beams or the shape of some contours, we frequently have more than two crossover points per contour.

We observe large biases (tens of centimeters to tens of meters) between GEDI data from different dates of acquisition. For simplicity, we only select for each lake the acquisition date giving the most complete H-A curve. Most of the time, it results in selecting the latest acquisition date of the dry season.

2.3.4 Matching water surface height with water surface area measurements

This method uses water surface height data and combines them with synchronous water surface area observations. To construct the height-area relationship, we search for the

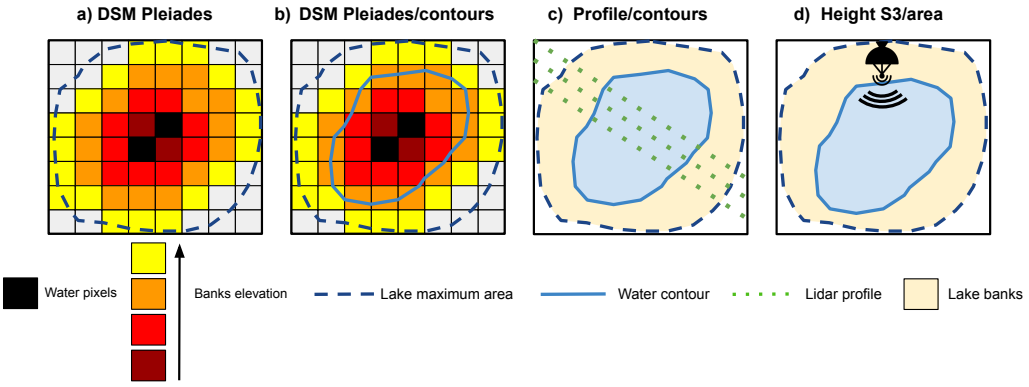

Figure 4. Schematic representation of the 4 methods used in this study to derive the height-area relationships.

Sentinel-2 images co-dated with the Sentinel-3 data and match the height and area measurements with a temporal tolerance of 3 days. A tolerance of 3 days is appropriate given the temporal variability of the lakes studied (De Fleury et al., 2023), and provides a good trade-off with respect to data availability. If the time difference between Sentinel-2 and Sentinel-3 acquisitions is not zero, we linearly interpolate successive water area data to the water surface height date. This method will be referred to as the "Height S3/area" method (Figure 4d).

2.4 Processing the height-area relationships

2.4.1 Processing the height-area relationships of in-situ data

For three reservoirs (Bam, Seytenga and Seguenega), in-situ data provided as H-V relationships have been converted to H-A relationships, computing the areas as the derivative of the volume with respect to the height A = dV/dH (Gao et al., 2012). For three lakes (Agoufou, Arzuma and Bangou Kirey), water surface height in-situ measurements are combined with Sentinel-2 water surface areas acquired on the same day. For Agoufou, since height data are acquired at a weekly frequency, Sentinel-2 areas are interpolated between two consecutive dates to match the in-situ data.

2.4.2 Resolving the bias between elevation data

As we do not have absolute elevation data for all methods, the comparison of the height-area relationships requires prior elevation bias removal. Indeed, the in-situ data and part of the Pleiades DSMs are not absolutely leveled, GEDI data showed acquisition time-dependent biases and the other remote sensing data have different references. The elevation biases are removed directly on the height-area curves. The DSM Pleiades/contours height-area method is taken as reference because it provides long and regular datasets, and the bias with the other methods is computed as the mean of the height differences:

$$bias = mean(h_{method} - h_{Pleiades})$$

2.4.3 Combining the height-area relationships based on open source data

The capabilities of the height-area relationships derived from methods based on open source data only have been also assessed. This concerns Profile ICESat-2/contours, Profile GEDI/contours and Height S3/area methods based on Sentinel-2 ICESat-2, GEDI and Sentinel-3 data.

For each lake, we fit the H-A relationship of the three methods combined with the best polynomial function of degree lower or equal to 2. Then, we discard the data outside the fit 95% confidence interval in order to remove the outliers. For the following, this method will be referred to as the "Combined open source" method.

2.5 Processing the volume-area relationships

For each height-area dataset associated with a specific lake and method, water volume changes are computed as the integral of the corresponding height-area function between two consecutive heights (Yao et al., 2023; Abileah et al., 2011). To do this, the H-A relationship is fitted and then integrated over H. A polynomial function (maximum degree of 5) is used for the fit and the Akaike Information Criterion (citeAkaike1973 is used to select the best fit and avoid overfitting. The volume-area relationship is finally given by cumulating volume changes. Since the height of the lake bottom is not always known, the reference is set to the "in-situ" data and all other methods are truncated to the minimum in-situ volume. Volumes from the different methods are then computed as relative volumes given by $V_{method} - V_{0,insitu}$. Moreover, since the different datasets do not start at the same water area, a dataset-specific volume offset called $V_{0,method}$ has to be resolved. The offset is computed as the mean difference with the in-situ dataset.

2.6 Methodology for the performance assessment of the different methods

Different metrics are used to assess the precision and accuracy of the different methods:

- Median Absolute Deviation

$$MAD = median(|y_i - median(y)|)$$

- Coefficient of determination

$$R^2 = 1 - \frac{\sum_{i=1}^{n}(y_i - \hat{y}_i)^2}{\sum_{i=1}^{n}(y_i - \bar{y}_i)^2}$$

- Root Mean Squared Difference

$$RMSD = \sqrt{\frac{1}{n}\sum_{i=0}^{n-1}(y_i - \hat{y}_i)^2}$$

- Normalized Root Mean Squared Difference

$$NRMSD = \frac{RMSD}{y_{max} - y_{min}}$$

- Root Mean Squared Error

$$RMSE = \sqrt{\frac{1}{n}\sum_{i=0}^{n-1}(y_i - y_{insitu})^2}$$

- Normalized Root Mean Squared Error

$$NRMSE = \frac{RMSE}{y_{insitu,max} - y_{insitu,min}}$$

where n is the number of observations, y_i the value observed by remote sensing, y_{insitu} the value observed in-situ, $\hat{y}_i$ the predicted value and $\bar{y}_i$ the mean value.

To assess the precision of the water heights retrieved by the different sources of elevation data, i.e. how flat these elevation data sources observe the water surface, we use the MAD because it is more robust to outliers than the standard deviation. The MAD is computed along the water transect for Sentinel-3 data and along the water contours estimated by Sentinel-2 for methods using Pleiades, ICESat-2 and GEDI data. For the last three methods, the dispersion estimate also includes water contour detection uncertainty and therefore does not allow a strict assessment of the precision of the water level data alone.

We provide information on the H-A curves dispersion using the R^2, height RMSD and height NRMSD of the A-H polynomial fits. The Normalized RMSD (NRMSD) is the RMSD divided by the amplitude of the height observations (y_{max}- y_{min}).

For the accuracy assessment of the heights and volumes, R^2, RMSE and NRMSE are used. Since lakes can have very different volumes, NRMSE provides a more comprehensive information compared to RMSE. in-situ H-A and A-V curves are interpolated to obtain height and volume matchups with data from the other methods.

3 Results

3.1 Height-area relationships

The height amplitude observed by the remote sensing-based methods is ranging from 1.5m (Agoufou, Bangui Mallam, Inbanta, Manga) to 4m (Arzuma, Toussiana), with most amplitudes below 3m (Figure 5). Fine shape patterns such as slope changes are well retrieved using the different methods and are in good agreement with in-situ data (e.g. Arzuma, Djigo, Kokorou, Tibin).

The methods relying on bank elevation data (Pleiades, ICESat-2 and GEDI) are dependent on the acquisition dates which limit the observable extent of the H-A curves. In the case of ICESat-2 data, the low number of data over the small lakes (Bangou Kirey, Manga, North Tanvi, South Tanvi) is also due to the fact that the laser beams only overpassed the lakes during the planned first two years of lidar mispointing. For Bangou Kirey, Pleiades, ICESat-2 and GEDI sensors overpassed the lake at a relatively high water level, not allowing exploring the full H-A curve. Conversely, simultaneous observations of in-situ water level and Sentinel-2-derived area are not available for the highest water levels, which occur for only a few days during the rainy season when cloud cover is a problem for optical imagery. Therefore, it remains difficult to compare in-situ and satellite estimates for this lake.

Complete drying of some lakes during the dry season increases the H-A curves extent but also introduces errors in the Pleiades DSM. Indeed the H-A relationships derived by the DSM Pleaides method show hockey cross patterns for Inbanta and North Tanvi. For these lakes which dried up, the water contour could not be used to estimate the starting altitude as described in Section 2.3.1, which has been set to 310m for Inbanta and 296m for North Tanvi. The presence of high noise in the DSM challenged other solutions to derive the starting altitude, such as for example using the minimum DSM elevation within the lake polygon. The location of the noisy DSM pixels is confirmed by areas of low pixel correlations corresponding to smooth surfaces such as, for instance, the lake bottom for North Tanvi (Figure 6). The noise leads to troughs several meters deep which force the starting altitude (lake bottom) to be underestimated. These pixels are filled progressively with small changes in lake area, which explains the observed hockey cross pattern. As soon as the lake is not completely dry, the average elevation computed over the smallest water area smoothes the noise and gives a correct minimum water elevation. For Inbanta, we also note a difference between the DSM Pleiades and the DSM Pleiades/contours curves reflected by overestimated water areas within the two first thirds of the DSM Pleiades curve. This

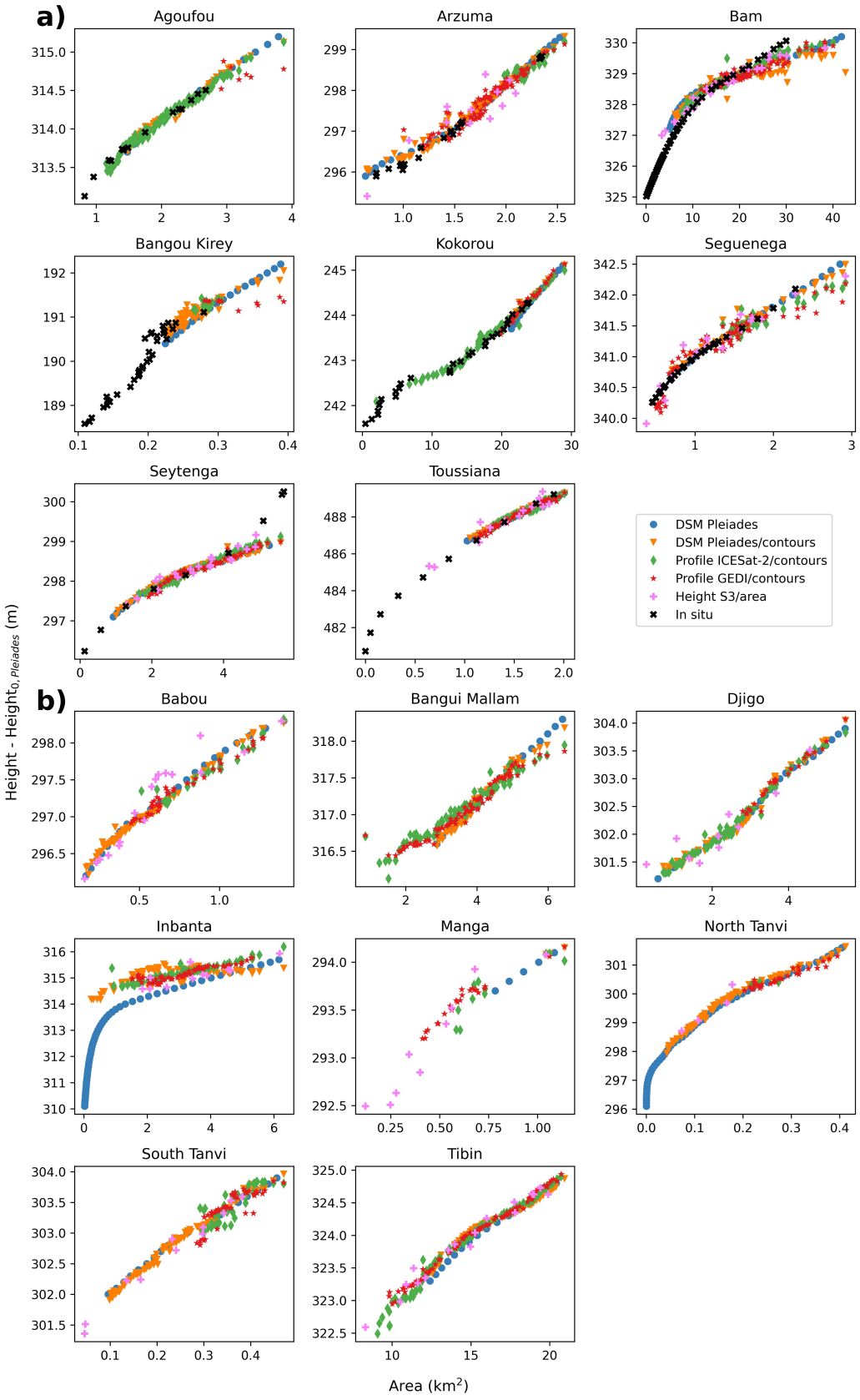

Figure 5. Height-area relationships derived from all the methods a) over the lakes with in-situ data and b) over the other lakes.

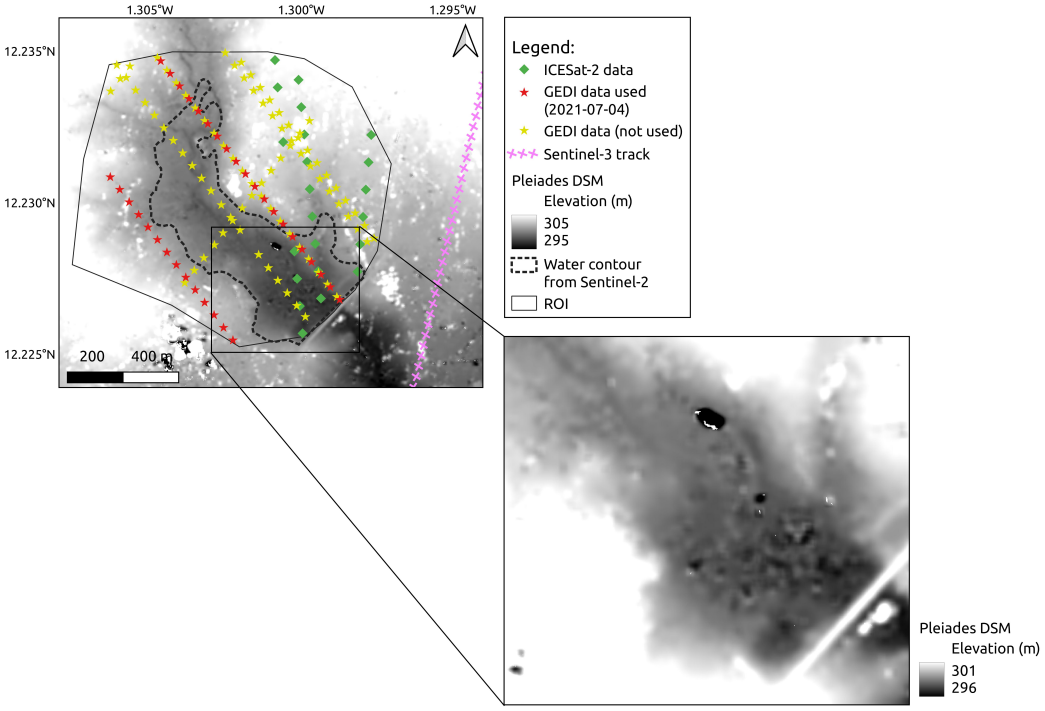

Figure 6. Data available over North Tanvi reservoir. We show a zoom on Pleiades DSM pixels over the bottom of the reservoir. The amplitude of the DSM noise exceeds 1.5m in some places.

difference is also attributed to the DSM noise, the resulting troughs causing a substantial quantity of pixels to be prematurely filled.

3.2 Volume-area relationships

The V-A curves also denote a generally good agreement between the different methods (Figure 7). Some small slope differences observed on the H-A curves comparison are more evident on the volume-area curves (e.g. DSM Pleiades over Kokorou lake), which is partly due to error propagation in the calculations. The largest differences with respect to in-situ data are observed over Bam and Seytenga reservoirs, where all remote sensing methods agree well with each other and differ from in-situ data. Part of these discrepancies may be due to bank erosion and sedimentation (Cecchi et al., 2020), with sediment transfer from the lake edge mainly due to land use (Tully et al., 2015) and wave-induced bank erosion (Hilton, 1985). For example, Boena and Dapola (2001) documented the Bam reservoir silting and showed that the sediment deposits in the lake could be of substantial thickness.

3.3 Quantitative results

3.3.1 Dispersion of the area-height relationship

All methods provided good fit results with almost all R^2 above 0.80 and most values above 0.90 (Table 2). The DSM Pleiades method outperforms all the other methods with all RMSD values below 0.03m, except for two lakes (Inbanta and North Tanvi) where RMSD equals 0.21m and 0.15m, respectively. The DSM Pleiades/contours, Profile ICESat-2/ and Profile GEDI/contours methods show good and consistent results with all RMSD values below 0.14m, most being below 0.10m. The Height S3/area method tends to produce curves

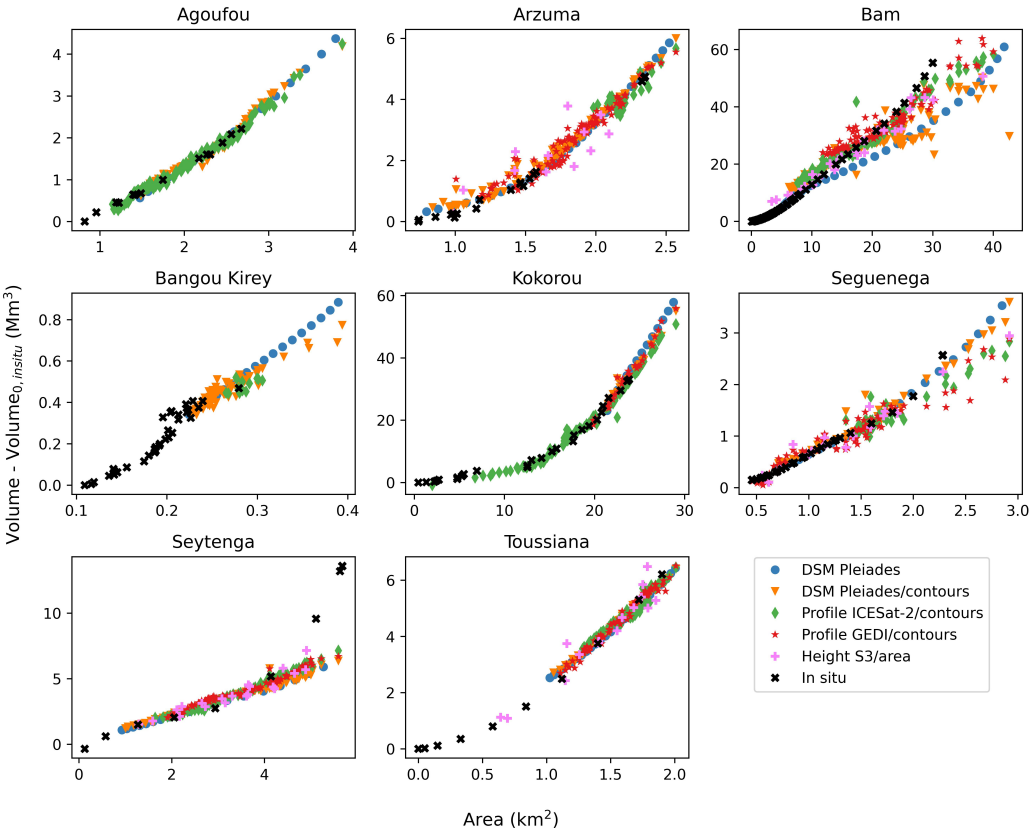

Figure 7. Volume-area relationships derived from the different methods over the lakes with in-situ data.

with dispersion values almost systematically greater than those from other methods. RMSD is between 0.09m and 0.34m, with 4 lakes having RMSD above 0.20m. A small part of this dispersion is inherently related to the time interpolation required to match water surface height and area measurements.

3.3.2 Precision of water elevation

The median MAD obtained using the different sources of elevation data (Figure 8) are respectively between 0.11m and 0.70m with most values below 0.20m for Pleiades, between 0.04m and 0.19m with most values below 0.13m for ICESat-2, between 0.04m and 0.23m with most values below 0.13m for GEDI, and between 0.01m and 0.12m with most values below 0.06m for Sentinel-3. Therefore, all sources of elevation data provide good results.

The number of points per contour/transect used to compute the precision varies with the methods and highly depends on lake size and, especially for Sentinel-3, and on the satellite's track attack angle with respect to the lake banks. The median number of points per contour ranges from 675 (Babou) to 4260 (Tibin) for Pleiades DSMs, from 2 (North Tanvi) to 50 (Bam) for ICESat-2, from 2 (Bangou Kirey) to 20 (Tibin) for GEDI (mainly because we selected only one acquisition date)and from 1 (Toussiana) to 12 (Bam) per transect for Sentinel-3.

The relatively low precision of Pleiades DSMs (> 0.40m) over certain lakes can be explained either by high amplitudes of noise due to very smooth areas or by flooded vegetation and trees. It is not surprising that the precision of Pleiades is poorer than other data sources, as we have chosen to generate the DSMs at a spatial resolution of 1m x 1m, which introduces more pixel-to-pixel noise than a coarser resolution. The average precision of 0.04m for Sentinel-3 must be taken carefully because for half of the lakes, the transects are made of a median number of 3 points or less. Except for these cases, all sources of data show a good precision stability with Inter-Quartile Ranges (IQR) < 0.20m.

3.3.3 Height-area and volume-area relationships accuracy

For all methods, the height RMSE is between 0.03m and 0.42m with most values below 0.30m and the height NRMSE is between 1.3% and 13.7% with most values below 8%. Some methods are missing for some lakes. They all perform well on the common lakes but not similarly from one lake to another. However, we do not observe systematic differences between one method and another. Heights derived from Sentinel-3 give higher RMSE and NRMSE on certain lakes. One of the reasons might be that radar altimeter waveforms are affected by crops or other water bodies surrounding the reservoir that generate relatively high backscattering (Arzuma). The other reason is the limitation of the radar altimeter along-track resolution. This can occur with small water bodies (noise observed for Babou and Manga lakes) or larger water bodies whose orientation with respect to the altimeter ground track generates narrow transects (Toussiana). Since these transects are made of very few measurements, they are more likely to provide larger errors.

For all methods, the volume RMSE is between 0.03Mm^3 and 8.72Mm^3 with most values below 5Mm^3 and the volume NRMSE is between 2.3% and 15.8% with most values below 11% (Table 3 and Figure 9). Similarly to the height statistics, we do not observe systematic differences between one method and another, or between one lake and another. Nevertheless, Profile GEDI/contours and Height S3/area methods are particularly impacted by some higher RMSEs due to the dispersion in the volume-area curve. In addition, some poor performances have been improved when going from height to volume accuracy, whereas some good performances have been reduced. This observation reflects that volume accuracy is not only a matter of height-area relationship accuracy and dispersion, but also a matter of height-area shape. This statement is supported by the results over Toussiana reservoir, where the difference between the Height S3/area method and the others methods are much

Table 2. Polynomial fit statistics of the area-height relationships.

	DSM Pleiades	DSM Pleiades/contours	Profile ICESat-2/contours	Profile GEDI/contours	Height S3/area
	Polynomial degree / R^2 / RMSD (m) / NRMSD (%)				
Agoufou	5 / > 0.99 / < 0.01 / 0.04	5 / 0.99 / 0.02 / 1.32	4 / 0.99 / 0.04 / 2.1	5 / 0.98 / 0.02 / 0.92	
Arzuma	5 / > 0.99 / 0.01 / 0.23	3 / 0.99 / 0.08 / 2.04	5 / 0.8 / 0.09 / 2.26	4 / 0.96 / 0.12 / 3.17	1 / 0.81 / 0.34 / 8.59
Babou	5 / > 0.99 / 0.01 / 0.62	5 / > 0.99 / 0.03 / 1.36	5 / 0.98 / 0.05 / 2.23	5 / 0.98 / 0.05 / 2.21	4 / 0.96 / 0.12 / 5.58
Bam	5 / > 0.99 / 0.03 / 0.82	5 / 0.95 / 0.12 / 3.82	5 / 0.97 / 0.09 / 2.93	4 / 0.93 / 0.1 / 3.14	2 / 0.98 / 0.1 / 3.23
Bangou Kirey	5 / > 0.99 / < 0.01 / 0.09	2 / 0.9 / 0.09 / 5.25	1 / 0.31 / 0.08 / 4.61	4 / 0.87 / 0.03 / 1.52	
Bangui Mallam	5 / > 0.99 / 0.01 / 0.4	5 / 0.98 / 0.07 / 2.37	5 / 0.97 / 0.08 / 2.78	5 / 0.99 / 0.05 / 1.91	
Djigo	5 / > 0.99 / 0.03 / 1.06	5 / 0.99 / 0.07 / 2.31	5 / 0.99 / 0.07 / 2.3	5 / 0.97 / 0.07 / 2.58	5 / 0.96 / 0.13 / 4.48
Inbanta	5 / 0.98 / 0.21 / 3.36	3 / 0.8 / 0.14 / 2.36	5 / 0.96 / 0.07 / 1.18	5 / 0.94 / 0.07 / 1.13	1 / 0.68 / 0.24 / 3.88
Kokorou	5 / > 0.99 / < 0.01 / 0.03	1 / 0.98 / 0.04 / 1.46	5 / 0.98 / 0.08 / 2.48	5 / 0.94 / 0.1 / 3.33	
Manga	5 / > 0.99 / < 0.01 / < 0.01	4 / > 0.99 / < 0.01 / < 0.01	2 / 0.91 / 0.08 / 4.91	5 / 0.99 / 0.03 / 1.61	3 / 0.97 / 0.09 / 5.64
North Tanvi	5 / 0.99 / 0.15 / 2.63	4 / 0.99 / 0.06 / 1.17	5 / > 0.99 / < 0.01 / < 0.01	3 / 0.92 / 0.09 / 1.61	5 / > 0.99 / < 0.01 / < 0.01
Seguenega	5 / > 0.99 / 0.01 / 0.34	2 / 0.98 / 0.06 / 2.14	1 / 0.84 / 0.09 / 3.6	5 / 0.95 / 0.11 / 4.36	4 / 0.95 / 0.13 / 4.97
Seytenga	3 / > 0.99 / 0.01 / 0.25	4 / 0.99 / 0.04 / 1.92	5 / 0.99 / 0.03 / 1.58	5 / 0.94 / 0.09 / 4.23	3 / 0.94 / 0.1 / 4.9
South Tanvi	5 / > 0.99 / 0.01 / 0.44	5 / 0.99 / 0.05 / 1.91	3 / 0.82 / 0.12 / 4.43	3 / 0.85 / 0.11 / 4.1	1 / 0.93 / 0.2 / 7.53
Tibin	5 / > 0.99 / < 0.01 / 0.05	5 / > 0.99 / 0.02 / 0.63	5 / 0.99 / 0.06 / 2.32	5 / 0.99 / 0.04 / 1.57	2 / 0.97 / 0.1 / 4.02
Toussiana	5 / > 0.99 / 0.01 / 0.12	4 / > 0.99 / 0.03 / 0.79	4 / 0.97 / 0.09 / 2.17	2 / 0.99 / 0.07 / 1.8	1 / 0.94 / 0.3 / 7.3

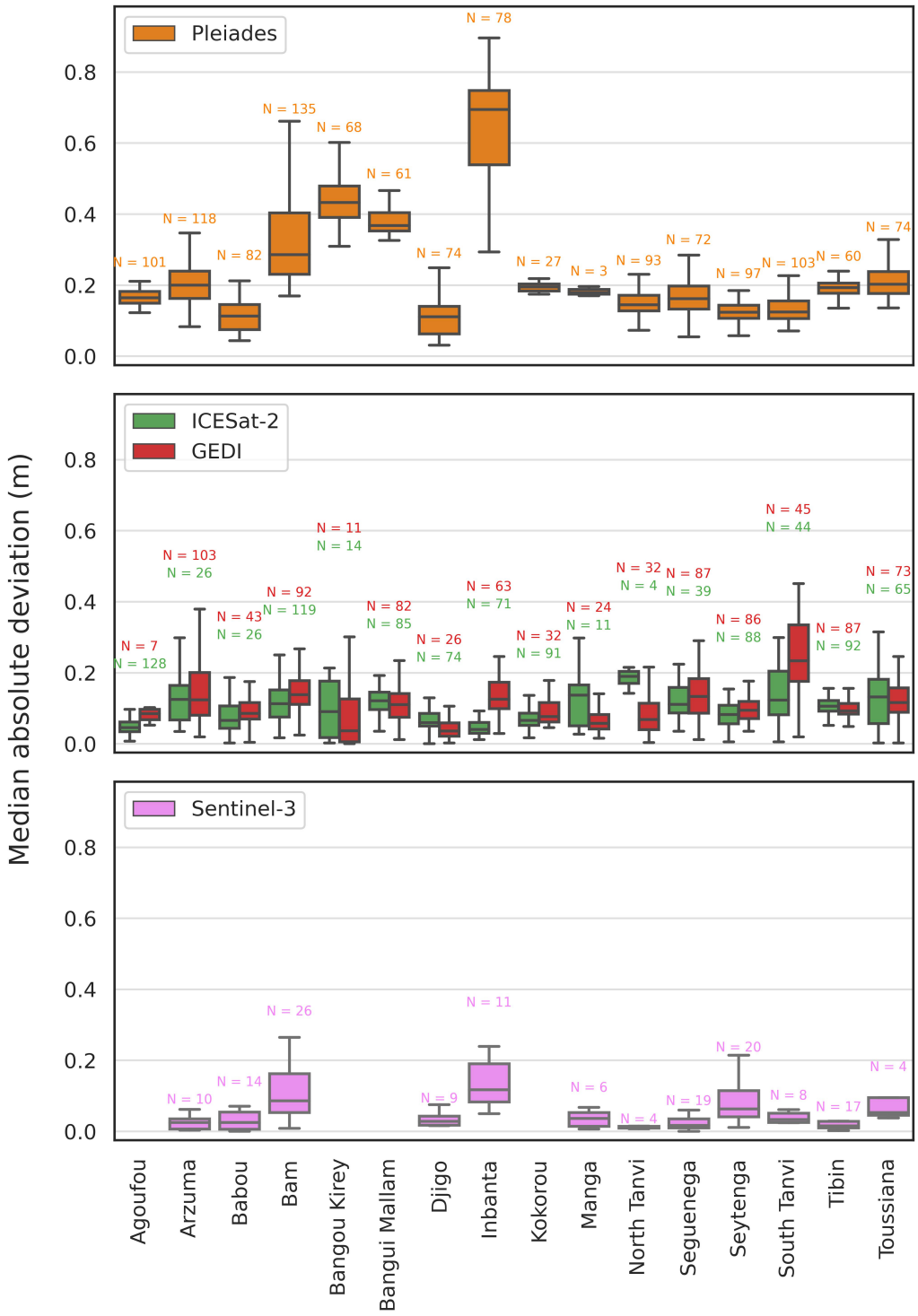

Figure 8. Box plot of the water elevation precision achieved by the different data sources. For each lake in x-axis, we plot the distribution of the water elevation precision in y-axis. The precisions computed for each transect/contour are stacked into a box reflecting the 25th, 50th and 75th percentiles of the distribution. Water elevations resulting from only one measurement are rejected.

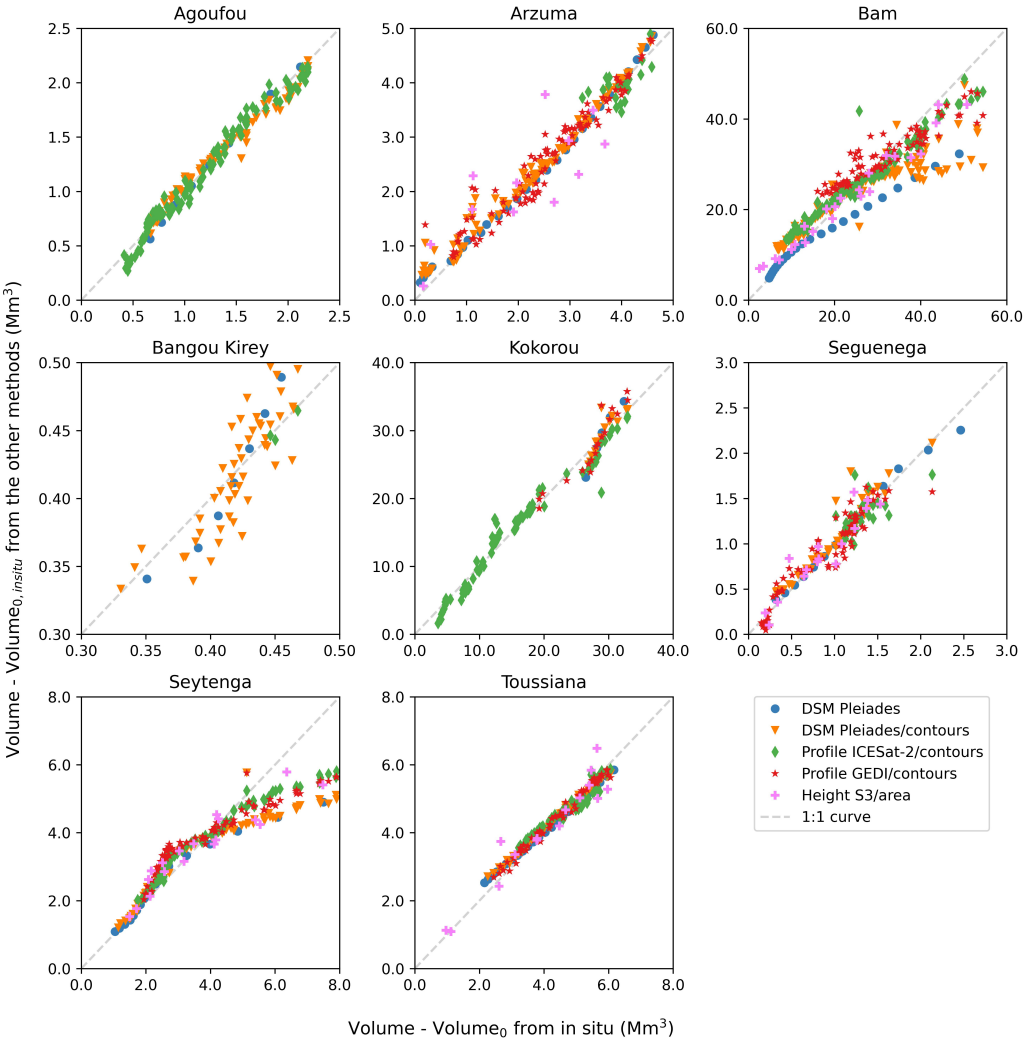

Figure 9. Comparison between relative volumes from in-situ (x-axis) and from other methods (y-axis). The 1:1 curve is plotted as grey dashed line.

lower when looking at the volume accuracy than the height accuracy metrics. We think that this is mainly due to the shape of the Height S3/area-derived height-area relationship that allows the volume-area relationship to fit the in-situ data more closely (Figure 5).

Table 3. Accuracy statistics of height and volume.

	DSM Pleiades	DSM Pleiades/contours	Profile ICESat-2/contours	Profile GEDI/contours	Height S3/area	Combined open source
			– Height –			
			R^2 / RMSE (m) / NRMSE (%)			
Agoufou	> 0.99 / 0.03 / 2.31	0.98 / 0.04 / 2.62	0.97 / 0.05 / 3.64			0.97 / 0.05 / 3.64
Arzuma	0.99 / 0.09 / 3.11	0.98 / 0.13 / 4.38	0.32 / 0.15 / 5.13	0.92 / 0.17 / 5.85	0.68 / 0.4 / 13.73	0.94 / 0.15 / 5.11
Bam	0.98 / 0.42 / 8.33	0.91 / 0.35 / 6.86	0.96 / 0.21 / 4.15	0.87 / 0.3 / 5.87	0.98 / 0.28 / 5.49	0.96 / 0.25 / 4.93
Bangou Kirey	0.93 / 0.19 / 7.63	0.66 / 0.11 / 4.2	0.48 / 0.23 / 8.93			0.48 / 0.23 / 8.93
Kokorou	0.96 / 0.17 / 6.49	0.73 / 0.07 / 2.56	0.96 / 0.11 / 3.97	0.87 / 0.09 / 3.27		0.98 / 0.08 / 3.13
Seguenega	> 0.99 / 0.03 / 1.43	0.94 / 0.07 / 3.84	0.37 / 0.11 / 5.64	0.92 / 0.14 / 7.27	0.88 / 0.14 / 7.43	0.93 / 0.11 / 5.95
Seytenga	0.95 / 0.27 / 6.23	0.9 / 0.28 / 6.57	0.94 / 0.22 / 5.24	0.91 / 0.27 / 6.28	0.92 / 0.18 / 4.18	0.93 / 0.24 / 5.72
Toussiana	> 0.99 / 0.17 / 1.96	> 0.99 / 0.12 / 1.43	0.95 / 0.16 / 1.91	0.99 / 0.11 / 1.27	0.94 / 0.32 / 3.76	0.98 / 0.14 / 1.7
			– Volume –			
			R^2 / RMSE (Mm^3) / NRMSE (%)			
Agoufou	> 0.99 / 0.05 / 2.37	0.98 / 0.08 / 3.51	0.98 / 0.08 / 3.77			0.98 / 0.16 / 7.23
Arzuma	0.99 / 0.14 / 2.99	0.98 / 0.2 / 4.27	0.32 / 0.3 / 6.37	0.93 / 0.28 / 5.86	0.62 / 0.71 / 14.97	0.94 / 0.27 / 5.79
Bam	0.99 / 6.25 / 11.29	0.85 / 6.71 / 12.11	0.95 / 3.79 / 6.85	0.87 / 4.91 / 8.87	0.97 / 3.43 / 6.2	0.95 / 8.72 / 15.75
Bangou Kirey	0.94 / 0.03 / 5.47	0.66 / 0.03 / 5.74	0.48 / 0.03 / 7.23			0.48 / 0.04 / 8.86
Kokorou	0.96 / 1.99 / 6.03	0.73 / 1.56 / 4.71	0.96 / 1.75 / 5.29	0.87 / 1.92 / 5.79		0.98 / 1.4 / 4.23
Seguenega	0.99 / 0.07 / 2.83	0.91 / 0.12 / 4.72	0.37 / 0.17 / 7.0	0.9 / 0.15 / 6.03	0.87 / 0.16 / 6.27	0.9 / 0.17 / 6.84
Seytenga	0.92 / 1.55 / 11.11	0.87 / 1.6 / 11.46	0.93 / 1.33 / 9.49	0.91 / 1.43 / 10.25	0.9 / 1.0 / 7.15	0.92 / 1.43 / 10.23
Toussiana	> 0.99 / 0.22 / 3.6	> 0.99 / 0.17 / 2.78	0.95 / 0.24 / 3.89	0.99 / 0.16 / 2.51	0.92 / 0.46 / 7.37	0.97 / 0.45 / 7.31

3.4 Combining all height-area curves from open source data

When combining the methods based on open source data (Figure 10), the results give height RMSE between 0.05m and 0.25m and height NRMSE between 1.7% and 8.9% with most values below 6%. The volume RMSE is between 0.04Mm^3 and 8.72Mm^3 with most values below 1.44Mm^3, and the volume NRMSE is between 4.2% and 15.8% with most values below 10.3% (Table 3). Except for a few lakes, these results are comparable to that obtained with the Profile ICESat-2/contours method alone.

4 Discussion

4.1 Comparison with the literature

4.1.1 Precision and accuracy of the area-height relationships

Many publications (Schwatke et al., 2020; Busker et al., 2019; Li et al., 2020; Chen et al., 2022) show similar results to those shown in 3.3.1 about the dispersion in the area-height relationships, and reported high values of R^2 (> 0.90). This is expected as water surface height and area are correlated. Our results with the Height S3/area method (RMSD values between 0.09m and 0.34m, with average being 0.16m) are slightly better that those of

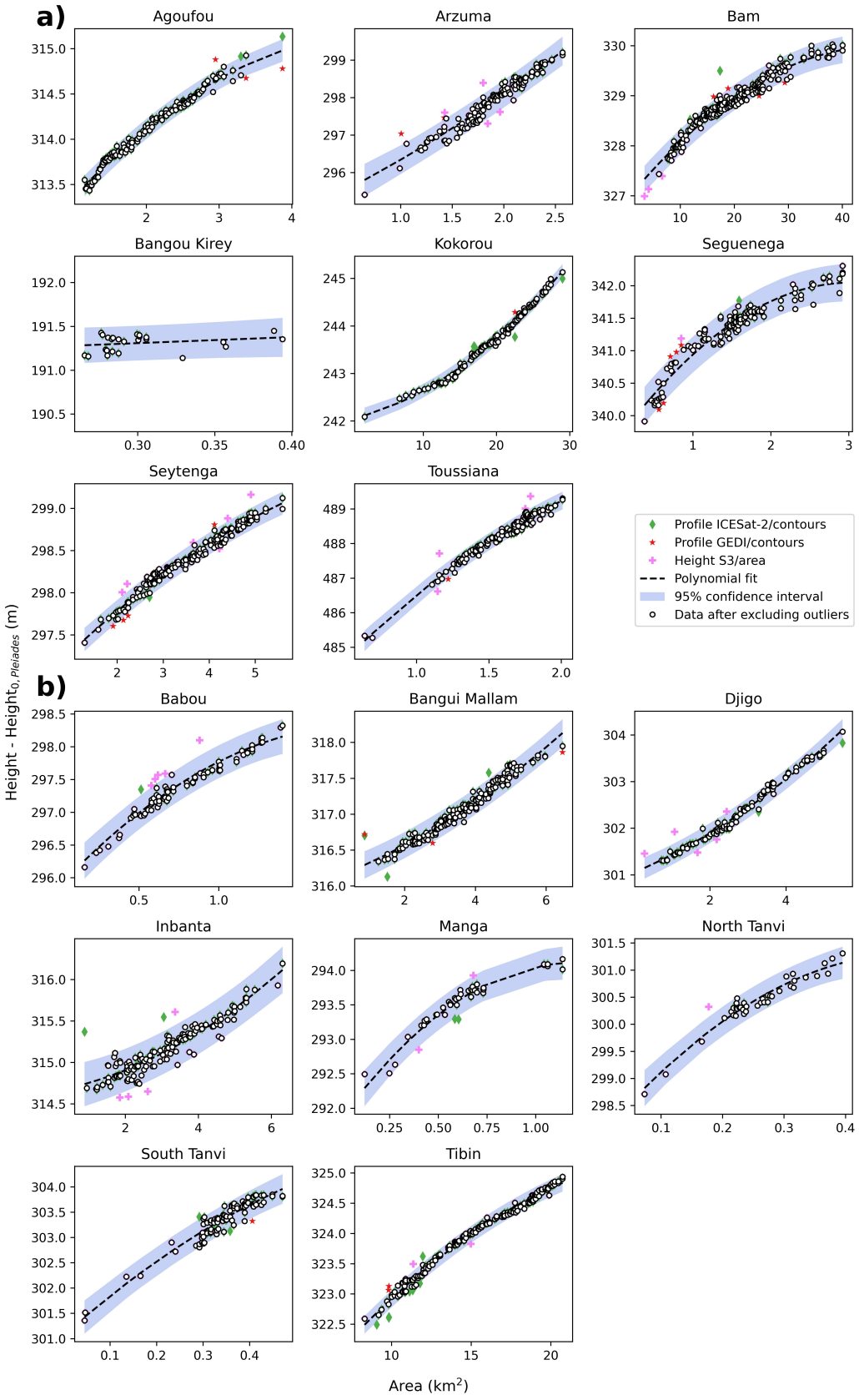

Figure 10. Combination of height-area curves from ICESat-2-, GEDI- and Sentinel-3-based methods for a) lakes with in-situ data and b) other lakes.

Schwatke et al. (2020) who reported RMSD values between 0.15m and 0.53m, and average of 0.27m, over 6 Texan lakes having a number of points comparable to that of our curves (e.g 32 points or less). Schwatke et al. (2020) used altimetry data from multiple missions with different accuracy, allowed a time lag of up to 10 days between water surface height and area data acquisitions, and did not perform time interpolation to generate the matchups, which may cause slightly larger RMSD.

Regarding the height-area relationship accuracy, most RMSE values are below 0.30m. Li et al. (2020) obtained RMSE values of 0.06m, 0.47m, 0.76m and 1.20m over four medium-sized lakes (1-100km^2) when validating their height-area curves derived from the combination of either ICESat, Hydroweb (`https://hydroweb.theia-land.fr`) (Crétaux et al., 2011) or G-REALM (`https://ipad.fas.usda.gov/cropexplorer/global_reservoir/`) (Birkett et al., 2011) altimetry data with water areas from the Joint Research Center (JRC) Global Surface Water (GSW) dataset (Pekel et al., 2016). Part of the difference with our results may be explained by elevation biases between remote sensing and in-situ data reported in the study of Li et al. (2020).

4.1.2 Precision of the height estimations

The water elevation precision along lake contours has been assessed in Section 3.3.2, with values ranging between 0.04m and 0.19m, and most values below 0.13m. Five lakes show a precision better or equal to 0.08m. These values are in line with Arsen et al. (2013) who reported water contour elevation standard deviations ranging from 0.02m to 0.11m when intersecting ICESat 170m posting rate banks elevation profiles with water contours over lake Poopo in Bolivia.

For GEDI, we did not find assessment of the water elevation precision along contour lines in the literature. If we compare the water contour elevation precision with values obtained along transects over water from other publications, our results (precision between 0.04m and 0.23m, with most values below 0.13m) are in line with Z. Zhang et al. (2023) who studied the water level dynamics of Qinghai Lake with GEDI data. The large biases noted on GEDI profiles from different acquisition dates were also pointed out by Fayad et al. (2020), and require further investigations.

For Sentinel-3, Taburet et al. (2020) reported a median standard deviation of water elevation of 0.17m. This is consistent but slightly higher than our results, which is expected as Taburet et al. (2020) studied thousands of water bodies, including rivers. Also, the use of the median absolute deviation in our study provides better results compared to using the standard deviation. More generally, standard deviations of a few centimeters have already been achieved over larger lakes with radar altimeters previous to Sentinel-3 (Crétaux & Birkett, 2006). This study shows that such a performance can be achieved on small and medium-sized lakes as well.

4.1.3 Water area estimations

The MNDWI threshold for water classification has been determined ad hoc for each lake. Using the same spectral index, we also tested automatic methods based on histogram analysis such as Otsu (Otsu, 1979) and Minimum Error Thresholding (Kittler & Illingworth, 1986). Both methods assume that the MNDWI distribution is bi-modal with two classes respectively associated with land and water. The Otsu's method determines the optimal threshold as the value which maximizes the inter-class variance and the MET method assumes that the histogram is a mixture of two gaussian-like distributions associated with the respective classes. Both methods were found to perform poorly in particular for lakes covered by aquatic vegetation (tri-modal histograms) or for lakes almost dried out (monomodal histograms for some dates). Consequently, we decided to follow De Fleury et al. (2023) and use ad hoc MNDWI thresholding. For some lakes, fairly negative threshold values have been

selected to account for aquatic vegetation (Table S1). We acknowledge that spatio-temporal variations in spectral signature of the lake or atmospheric conditions may lead to underestimation or overestimation of the water surface area, but ad hoc thresholding allows for a more consistent time series. The accuracy of the water surface areas has not been directly assessed but the results of Section 3.3.2 indicate that the precision of the water contours elevation is of the order of 0.10m to 0.20m. This, combined with the satisfactory height-area relationships dispersion and accuracy, reflects a good water contours detection accuracy and proves ad hoc MNDWI thresholding to be efficient for our study.

4.1.4 Accuracy of the volume-area relationships

We reported volume NRMSE between 2.3% and 15.8%, with most values below 11%. This is in line with Busker et al. (2019) who validated volume variations derived from the combination of radar altimetry and GSW monthly areas over 18 global lakes and reservoirs and obtained NRMSE between 1.784% and 18.872% with most values below 11% (extrapolated volumes excluded). Schwatke et al. (2020) also obtained similar results with NRMSE (defined as the RMSE divided by the difference of the 95% percentile and the 5% percentile of the height variations) varying between 2.8% and 14.9%, with an average of 8.3%, when validating against in-situ volume variations. The in-situ data used in our study come from various sources (with errors difficult to estimate) and may induce different uncertainties during the comparisons.

4.2 Pros and cons of each method

4.2.1 Pleiades-based methods

Pleiades-based height-area relationships show generally good performance in terms of accuracy, water elevation precision and dispersion. In particular, those derived from the DSM Pleiades method have the advantage of relying on a single data source. However, our study shows that despite their very high spatial resolution, Pleiades DSMs should be subjected to preliminary quality checks for issues related to jitter and high noise due to low pixel correlation, which can introduce errors of several meters. Dried out lake Pleiades DSMs allow characterizing the topography of the whole lake bathymetry but also represent a challenge for the estimation of the lake bottom altitude. Indeed in the absence of water, determining the starting altitude of the height-area relationship is not straightforward as the lake bottom may show high noise. In this study we manually selected a starting altitude from which water areas increase significantly. Alternative options might be to use the elevation from an external water contour intersected with the DSM, or to correct for the amplitude of the noise estimated over a flat area. If the noise is more widely spread over the banks (not only on the lake bottom but also on higher parts of the banks), reducing the starting altitude is mandatory in order not to underestimate the water areas subsequently computed.

The DSM Pleiades/contours method, which combines Pleiades DSMs with water contours, requires an additional data source compared to the DSM Pleiades method but is not affected by the effect of dry lake noise on the starting elevation of the curves, as these are truncated to the minimum water contour extent. More generally, Pleiades DSMs represent the surface elevation, and thus remain affected by all kinds of relief such as vegetation whose footprint on the DSMs is often wider due to smoothing in the DSM generation processing.

4.2.2 Lidar-based methods

Profile ICESat-2/ and Profile GEDI/contours methods are able to generate accurate height-area relationships over small to medium-sized lakes with sometimes a single but more often a few numbers of bank elevation profiles. Furthermore, these relationships are consistent with very high resolution DSM-based curves and highlight the potential of existing lidar altimetry missions for lake volume changes monitoring. We also note that the satis-

factory water elevation precision obtained with ICESat-2 and GEDI data suggests that the algorithm implemented in the respective operational products used in this study properly separate echos from tree canopy and ground. Nonetheless, the methods face some limitations. Among them, the height-area relationship quality depends on the lake's shape and the attack angle of the lidar altimeter ground tracks with respect to the water contours. The more parallel to the lake the trajectory is, the bigger the impact of water detection errors on the resulting contour elevation will be. The location of the lidar profiles is important as well since it also conditions the sensitivity of the methods to water detection errors (as it could be the case for dendritic lakes or profiles located close to the shore). The lidar data posting rates of respectively 60m and 100m represent a limitation with respect to the range of bank slope that can be observed. A threshold on the bank slope must be applied to prevent errors induced by linear interpolation of the topography or water detection which is more challenging as the banks get steeper. Another limitation of ICESat-2 (nominal revisit time of 91 days, drifting orbit during the first two years of the mission) and GEDI (variable revisit time) data is the temporal coverage which conditions the observable volume dynamics. In addition, GEDI suffers from some degraded acquisition periods (Urbazaev et al., 2022). Finally, being optical sensors, lidars are not suited to areas with important cloud cover. In this study we were not significantly impacted by this effect as the dry season, with very low or absent cloud cover, represents the major part of the year in the study area.

4.2.3 Height S3/area method

As well as lidar data, Sentinel-3 data are less impacted by relief than the Pleiades DSMs and better separate water from flooded vegetation, as suggested by the comparison between Height S3/area and Pleiades-based height-area relationships over the Inbanta lake. One of the advantages of Sentinel-3 data, in addition to having no trouble with cloud cover, is also the temporal coverage (revisit time of 27 days) which excldues the acquisition dates dependency associated with the other methods and may allow observing a greater water volume dynamics. Even more frequent revisit time is possible with Sentinel-6 data (10 days) but the spatial coverage decreases substantially (e.g. only one of the lakes studied is covered by Sentinel-6). Nonetheless, despite good water surface height precision (below 0.10m for most lakes), the Height S3/area method tends to generate height-area relationships with more dispersion (Section 3.3.1). In addition to the impact of time interpolation for matching S2 and S3 data, part of these errors might be attributed to contamination of the radar waveform by surrounding bright surfaces such as crops, humid soils or neighboring water bodies which challenge the retracking (Boy et al., 2022).

4.3 Learnings from this study

4.3.1 Characterization of small and shallow water bodies

Overall, the methods were able to derive consistent height-area relationships of small and medium-sized lakes with areas ranging from tens of hectares to tens of square kilometers and small height amplitudes about 1.5m. This result represents a step forward for volume change monitoring of shallow lakes. Indeed, multiple publications in the literature focus on lakes with higher water level amplitude or use 1m-vertical resolution DEM such as SRTM data to estimate height-area relationships or volume changes (Fang et al., 2019; S. Zhang & Gao, 2020; Pan et al., 2013; Yao et al., 2018).

The slope breaks and curvatures consistently observed on the height-area relationships of some lakes such as Djigo, Kokorou and Tibin (Figure 5) are of particular interest as they reveal fine shape behaviors. Since multiple existing studies (Gao et al., 2012; Crétaux et al., 2015; Busker et al., 2019; Smith & Pavelsky, 2009; S. Zhang & Gao, 2020; Bhagwat et al., 2019; Fang et al., 2019; Li et al., 2020; Chen et al., 2022), consider linear, quadratic or power-law regressions to fit the height-area relationship, our observations show that such

assumptions might be unsuited to capture complex shape patterns in the case of small and medium-sized lakes.

4.3.2 Spatial coverage and data accessibility

Pleiades images are commercial data, so they are not open-access. We tested the potential of open-access global DEMs such as SRTM data to produce height-area relationships. For this, the DEM filling method has been used on the SRTM DEM of each of the sixteen lakes studied. With the exception of the Tibin reservoir, which is among the largest studied lakes (mean area of 15.39km^2) and was not impounded yet during the SRTM acquisition, the resulting height-area relationships showed a general disagreement with all other methods as they were almost systematically steeper. Moreover, the 1-m vertical resolution of SRTM, as well as that of other global DEMs such as the ALOS Global Digital Surface Model (AW3D30) or the ASTER Global Digital Elevation Map (GDEM), is insufficient to capture water surface height variations of a few meters that we commonly observe. GLO-30 Copernicus DEM has a better vertical resolution but represents a 2011-2015 averaged topography from multiple DEMs derived from the TanDEM-X mission and acquired with different water levels. Hence, bank topography must be regarded carefully as it may contain contributions from water.

Due to the spatial coverage limitation of the conventional altimetry missions, none of the studied lakes are included in the global databases such as Hydroweb, G-REALM or the Database for Hydrological Time Series of Inland Waters (DAHITI, `https://dahiti.dgfi.tum.de/en`) (Schwatke et al., 2015). De Fleury et al. (2023) intersected Sentinel-3A and Sentinel-3B altimeter ground tracks with the lakes maximum water extent from GSW dataset over Central Sahel and estimated a total number of only 150 lakes below the tracks, which is far below the several thousands of water bodies found in the region by Pi et al. (2022). Moreover, the inter-track distance of other altimetry missions such as Sentinel-6 is larger than that of Sentinel-3. This emphasizes the limited spatial coverage of the radar altimeters.

Multi-beams lidar altimetry data from ICESat-2 and GEDI missions allows bypassing the limitations mentioned above by providing open-access surface elevation data with enhanced spatial coverage compared to that of radar altimetry missions. Indeed, Chen et al. (2022) showed for example that the ICESat-2 ATL13 product allowed observing 2 to 7 times more global water bodies than what the traditional altimetry missions can do. The ATL13 product being spatially limited by a shape mask derived from existing inland water bodies databases (Jasinski et al., 2023), it is likely that the ATL08 product used in our study allows for an even better spatial coverage.

4.3.3 Combination of methods based on open-access data

We showed that combining the methods based on non-commercial data gave results comparable to that obtained with the Profile ICESat-2/contours method alone, so the benefit in terms of accuracy is not substantial. However, combining different methods mitigates some of the limitations of each method and provides more robust curves. The temporal coverage (sub-monthly revisit time) of radar altimetry data and the spatial coverage of lidar data improve the height-area curves extent and the number of water bodies observed, respectively. Thus, the combination of radar and lidar altimetry data provides an open source solution for upscaling volume dynamics analysis to a wider range of lakes, as the methods are easily transferable to other lakes. This could be of particular interest for the monitoring of ungauged lakes or lakes with outdated in-situ data.

5 Conclusion

The height-area relationships of sixteen lakes and reservoirs in West Africa have been derived from four different methods. These methods used different data sources such as Pleiades DSMs, Sentinel-2 optical imagery, ICESat-2 and GEDI lidar altimetry and Sentinel-3 radar altimetry. We found a generally good agreement with in-situ data (most height RMSE values below 0.30m and volume NRMSE values below 11%) and among the methods. With the exception of the Sentinel-3-based method which tends to produce higher dispersions, all methods provide curves with very low noise (fit RMSD values below 0.10m for most lakes). Fine shape patterns were consistently observed over small height amplitudes, highlighting the ability of the different methods to monitor shallow lakes with non-linear bathymetric behaviors. We found satisfactory water elevation precisions, with values close to 0.20m using Pleiades DSMs and slightly better values of the order of 0.13m or less using the other methods. We identified inherent limitations in terms of data quality, surface features, spatio-temporal coverage and data accessibility. This analysis suggests that lidar-based methods combined with radar altimetry data show similar performance to high-resolution DSMs-based methods and therefore have great potential for estimating water volume changes over lakes and reservoirs in this region. Furthermore, benefiting from its wide-swath Ka-band radar interferometer (KaRIN), the Surface Water and Ocean Topography (SWOT) mission, launched on December 16, 2022, will be able to observe 90% of the inland areas and all lakes larger than 250 x 250m^2 (requirements) located between 78°N and 78°S (Biancamaria et al., 2016). With a minimum revisit time of 21 days, SWOT will thus provide volume change estimates for the majority of the lakes and reservoirs in the study area, further expanding the number of water bodies that could be addressed by remote sensing. The H-A-V relationships derived in this study will provide a valuable database to assess SWOT performances in this area.

Open Research Section

Data Availability

The in-situ water surface elevation data on Bangou Kirey and Agoufou lakes are available in the AMMA-CATCH observatory database (`www.amma-catch.org`, DOI: `https://doi.org/10.2136/vzj2018.03.0062`). For the height-volume relationships of Bam, Seguenega and Seytenga reservoir, please contact the Institut International d'Ingénierie de l'Eau et de l'Environnement (2IE, ousmane.yonaba@2ie-edu.org, tazen.fowe@2ie-edu.org). The height-area relationships of the Kokorou lake and Toussiana reservoir have been extracted respectively from Baba et al. (2019) and Sanogo and Dezetter (1997).

The Sentinel-2 L2A Surface Reflectance (SR) images are available on Google Earth Engine (GEE, (Gorelick et al., 2017)) as the "Sentinel-2 MSI: MultiSpectral Instrument, Level-2A" collection (`https://developers.google.com/earth-engine/datasets/catalog/COPERNICUS_S2_SR`). The Sentinel-3 Sar Radar Altimeter (SRAL) data and the Altimetric Time Series Software (AlTiS, (Frappart et al., 2021)) are provided by the Centre de Topographie des Océans et de l'Hydrosphère (CTOH, `https://www.legos.omp.eu/ctoh/catalogue/`). The Ice, Cloud and land Elevation Satellite-2 (ICESat-2) L3A Land and Vegetation height data product (ATL08) is accessible on the National Snow and Ice Data Center (NSIDC) website (`https://nsidc.org/data/atl08/versions/6`). The Global Dynamics Ecosystem Investigation (GEDI) L2A Geolocated Elevation and Height Metrics (GEDI02_A) are downloaded from the NASA Land Processes Distributed Active Archive Center (LP DAAC, `https://lpdaac.usgs.gov/products/gedi02_av002/`).

The dataset containing the height-area-volume relationships of the remote sensing-based methods is provided as a CSV file accessible through `https://dataverse.ird.fr/privateurl.xhtml?token=ac61adc6-254a-4ccc-9061-7a6d1bd21612`. The dataset also includes the in-situ data-based height-area-volume relationship of the Arzuma reservoir. In

order to allow a direct comparison, the provided relationships are all unbiased with respect to the DSM Pleiades method.

Acknowledgments

This work was supported by CNES through the APR program funding the SPLASH project, in the framework of the pre-launch activities related to the SWOT mission. Occitanie Region and Collecte Localisation Satellites (CLS) also supported this work by funding Félix Girard's PhD thesis. We acknowledge CNES and Airbus DS for providing the Pleiades images, and the AMMA-CATCH observatory for in-situ data supply in Niger and Mali. We are very grateful to Nicolas Taburet and Nicolas Picot for discussions on the altimetry data, to Etienne Berthier for sharing his expertise on DSM processing and analysis, to Guillaume Favreau for sharing his knowledge of water bodies in Niger, and to Jean-Marie Dipama for information on reservoirs in Burkina Faso.

References

Abileah, R., Vignudelli, S., & Scozzari, A. (2011). A completely remote sensing approach to monitoring reservoirs water volume. *Fifteenth International Water Technology Conference, IWTC 15 2011, Alexandria, Egypt*, 18.

Annor, F., Van De Giesen, N., Liebe, J., Van De Zaag, P., Tilmant, A., & Odai, S. (2009). Delineation of small reservoirs using radar imagery in a semi-arid environment: A case study in the upper east region of Ghana. *Physics and Chemistry of the Earth, Parts A/B/C*, *34*(4-5), 309–315. Retrieved 2023-09-02, from https://linkinghub.elsevier.com/retrieve/pii/S1474706508002222 doi: 10.1016/j.pce.2008.08.005

Arsen, A., Crétaux, J.-F., Berge-Nguyen, M., & del Rio, R. (2013). Remote Sensing-Derived Bathymetry of Lake Poopó. *Remote Sensing*, *6*(1), 407–420. Retrieved 2022-05-30, from http://www.mdpi.com/2072-4292/6/1/407 doi: 10.3390/rs6010407

Avisse, N., Tilmant, A., Müller, M. F., & Zhang, H. (2017). Monitoring small reservoirs' storage with satellite remote sensing in inaccessible areas. *Hydrology and Earth System Sciences*, *21*(12), 6445–6459. Retrieved 2022-10-05, from https://hess.copernicus.org/articles/21/6445/2017/ doi: 10.5194/hess-21-6445-2017

Baba, A., Maïga, O. F., Ousmane, B., Constant, D. D. E., & Favreau, G. (2019). Fonctionnement hydrologiquede la grande mare de kokorou dans le socle cristallin du liptako gourma (niger). *International Journal of Biological and Chemical Sciences*, *12*(6), 2951. Retrieved 2023-08-18, from https://www.ajol.info/index.php/ijbcs/article/view/183877 doi: 10.4314/ijbcs.v12i6.36

Bacalhau, J. R., Ribeiro Neto, A., Crétaux, J.-F., Bergé-Nguyen, M., & Moreira, D. M. (2022). Bathymetry of reservoirs using altimetric data associated to optical images. *Advances in Space Research*, *69*(11), 4098–4110. Retrieved 2022-07-08, from https://linkinghub.elsevier.com/retrieve/pii/S0273117722001971 doi: 10.1016/j.asr.2022.03.011

Bagnardi, M., González, P. J., & Hooper, A. (2016). High-resolution digital elevation model from tri-stereo pleiades-1 satellite imagery for lava flow volume estimates at fogo volcano. *Geophysical Research Letters*, *43*(12), 6267–6275. Retrieved 2023-11-10, from https://agupubs.onlinelibrary.wiley.com/doi/10.1002/2016GL069457 doi: 10.1002/2016GL069457

Bhagwat, T., Klein, I., Huth, J., & Leinenkugel, P. (2019). Volumetric analysis of reservoirs in drought-prone areas using remote sensing products. *Remote Sensing*, *11*(17), 1974. Retrieved 2023-10-11, from https://www.mdpi.com/2072-4292/11/17/1974 doi: 10.3390/rs11171974

Biancamaria, S., Lettenmaier, D. P., & Pavelsky, T. M. (2016). The SWOT Mission and Its Capabilities for Land Hydrology. *Surveys in Geophysics*, *37*(2), 307–337. Retrieved 2022-09-30, from http://link.springer.com/10.1007/s10712-015-9346-y doi: 10.1007/s10712-015-9346-y

Biggs, J., Von Fumetti, S., & Kelly-Quinn, M. (2017). The importance of small waterbodies for biodiversity and ecosystem services: implications for policy makers. *Hydrobiologia*, *793*(1), 3–39. Retrieved 2024-01-02, from http://link.springer.com/10.1007/s10750-016-3007-0 doi: 10.1007/s10750-016-3007-0

Birkett, C., Reynolds, C., Beckley, B., & Doorn, B. (2011). From research to operations: The usda global reservoir and lake monitor. *Coastal Altimetry*, 19-50.

Boena, C., & Dapola, E. (2001). *L'ensablement du lac bam : causes et conséquences.* Retrieved from https://beep.ird.fr/collect/depgeo/index/assoc/BOECYR01/BOECYR01.pdf

Boy, F., Cretaux, J.-F., Boussaroque, M., & Tison, C. (2022). Improving Sentinel-3 SAR Mode Processing Over Lake Using Numerical Simulations. *IEEE Transactions on Geoscience and Remote Sensing*, *60*, 1–18. Retrieved 2022-06-03, from https://ieeexplore.ieee.org/document/9656730/ doi: 10.1109/TGRS.2021.3137034

Busker, T., De Roo, A., Gelati, E., Schwatke, C., Adamovic, M., Bisselink, B., ... Cottam, A. (2019). A global lake and reservoir volume analysis using a surface water dataset and satellite altimetry. *Hydrology and Earth System Sciences*, *23*(2), 669–690. Retrieved 2023-11-10, from https://hess.copernicus.org/articles/23/669/2019/ doi: 10.5194/hess-23-669-2019

Carabajal, C. C., & Boy, J.-P. (2021). Lake and reservoir volume variations in South America from radar altimetry, ICESat laser altimetry, and GRACE time-variable gravity. *Advances in Space Research*, *68*(2), 652–671. Retrieved 2023-01-23, from https://linkinghub.elsevier.com/retrieve/pii/S027311772030260X doi: 10.1016/j.asr.2020.04.022

Cecchi, P., Forkuor, G., Cofie, O., Lalanne, F., Poussin, J.-C., & Jamin, J.-Y. (2020). Small Reservoirs, Landscape Changes and Water Quality in Sub-Saharan West Africa. *Water*, *12*(7), 1967. Retrieved 2023-06-08, from https://www.mdpi.com/2073-4441/12/7/1967 doi: 10.3390/w12071967

Cecchi, P., Meunier-Nikiema, A., Moiroux, N., & Sanou, B. (2009). Towards an Atlas of Lakes and Reservoirs in Burkina Faso. *Small reservoir toolkit*.

Chen, T., Song, C., Luo, S., Ke, L., Liu, K., & Zhu, J. (2022). Monitoring global reservoirs using ICESat-2: Assessment on spatial coverage and application potential. *Journal of Hydrology*, *604*, 127257. Retrieved 2023-12-21, from https://linkinghub.elsevier.com/retrieve/pii/S002216942101307X doi: 10.1016/j.jhydrol.2021.127257

Cooley, S. W., Ryan, J. C., & Smith, L. C. (2021). Human alteration of global surface water storage variability. *Nature*, *591*(7848), 78–81. Retrieved 2023-06-22, from https://www.nature.com/articles/s41586-021-03262-3 doi: 10.1038/s41586-021-03262-3

Crétaux, J.-F., Abarca-del Río, R., Bergé-Nguyen, M., Arsen, A., Drolon, V., Clos, G., & Maisongrande, P. (2016). Lake volume monitoring from space. *Surveys in Geophysics*, *37*(2), 269–305. Retrieved 2022-09-18, from http://link.springer.com/10.1007/s10712-016-9362-6 doi: 10.1007/s10712-016-9362-6

Crétaux, J.-F., Arsen, A., Calmant, S., Kouraev, A., Vuglinski, V., Bergé-Nguyen, M., ... Maisongrande, P. (2011). SOLS: A lake database to monitor in the near real time water level and storage variations from remote sensing data. *Advances in Space Research*, *47*(9), 1497–1507. Retrieved 2023-12-07, from https://linkinghub.elsevier.com/retrieve/pii/S0273117711000287 doi: 10.1016/j.asr.2011.01.004

Crétaux, J.-F., Biancamaria, S., Arsen, A., Bergé-Nguyen, M., & Becker, M. (2015). Global surveys of reservoirs and lakes from satellites and regional application to the syrdarya river basin. *Environmental Research Letters*, *10*(1), 015002. Retrieved 2023-06-13, from https://iopscience.iop.org/article/10.1088/1748-9326/10/1/015002 doi: 10.1088/1748-9326/10/1/015002

Crétaux, J.-F., & Birkett, C. (2006). Lake studies from satellite radar altimetry. *Comptes Rendus Geoscience*, *338*(14), 1098–1112. Retrieved 2023-12-21, from https://linkinghub.elsevier.com/retrieve/pii/S1631071306002318 doi: 10.1016/j.crte.2006.08.002

De Fleury, M., Kergoat, L., & Grippa, M. (2023). Hydrological regime of Sahelian small waterbodies from combined Sentinel-2 MSI and Sentinel-3 Synthetic Aperture Radar Altimeter data. *Hydrology and Earth System Sciences*, *27*(11), 2189–2204. Retrieved 2024-02-20, from https://hess.copernicus.org/articles/27/2189/2023/ doi: 10.5194/hess-27-2189-2023

Descroix, L., Guichard, F., Grippa, M., Lambert, L., Panthou, G., Mahé, G., ... Paturel, J.-E. (2018). Evolution of surface hydrology in the sahelo-sudanian strip: An updated review. *Water*, *10*(6), 748. Retrieved 2023-03-30, from http://www.mdpi.com/2073-4441/10/6/748 doi: 10.3390/w10060748

Duan, Z., & Bastiaanssen, W. (2013). Estimating water volume variations in lakes and reservoirs from four operational satellite altimetry databases and satellite imagery data. *Remote Sensing of Environment*, *134*, 403–416. Retrieved 2023-12-21, from https://linkinghub.elsevier.com/retrieve/pii/S0034425713000898 doi: 10.1016/j.rse.2013.03.010

Dubayah, R., Blair, J. B., Goetz, S., Fatoyinbo, L., Hansen, M., Healey, S., ... Silva, C. (2020). The global ecosystem dynamics investigation: High-resolution laser ranging of the earth's forests and topography. *Science of Remote Sensing*, *1*, 100002. Retrieved 2023-10-30, from https://linkinghub.elsevier.com/retrieve/pii/S2666017220300018 doi: 10.1016/j.srs.2020.100002

European Space Agency, S. (2021). *Copernicus global digital elevation model. distributed by opentopography.* Retrieved from https://doi.org/10.5069/G9028PQB doi: 10.5069/G9028PQB

Fang, Li, Wan, Zhu, Wang, Hong, & Wang. (2019). Assessment of water storage change in china's lakes and reservoirs over the last three decades. *Remote Sensing*, *11*(12), 1467. Retrieved 2023-10-12, from https://www.mdpi.com/2072-4292/11/12/1467 doi: 10.3390/rs11121467

Favreau, G., Cappelaere, B., Massuel, S., Leblanc, M., Boucher, M., Boulain, N., & Leduc, C. (2009). Land clearing, climate variability, and water resources increase in semiarid southwest Niger: A review. *Water Resources Research*, *45*(7), 2007WR006785. Retrieved 2024-01-29, from https://agupubs.onlinelibrary.wiley.com/doi/10.1029/2007WR006785 doi: 10.1029/2007WR006785

Fayad, I., Baghdadi, N., Bailly, J. S., Frappart, F., & Zribi, M. (2020). Analysis of GEDI elevation data accuracy for inland waterbodies altimetry. *Remote Sensing*, *12*(17), 2714. Retrieved 2023-06-02, from https://www.mdpi.com/2072-4292/12/17/2714 doi: 10.3390/rs12172714

Fowe, T., Karambiri, H., Paturel, J.-E., Poussin, J.-C., & Cecchi, P. (2015). Water balance of small reservoirs in the Volta basin: A case study of Boura reservoir in Burkina Faso. *Agricultural Water Management*, *152*, 99–109. Retrieved 2023-06-08, from https://linkinghub.elsevier.com/retrieve/pii/S0378377415000153 doi: 10.1016/j.agwat.2015.01.006

Frappart, F., Blarel, F., Fayad, I., Bergé-Nguyen, M., Crétaux, J.-F., Shu, S., ... Baghdadi, N. (2021). Evaluation of the performances of radar and lidar altimetry missions for water level retrievals in mountainous environment: The case of the swiss lakes. *Remote Sensing*, *13*(11), 2196. Retrieved 2023-01-23, from https://www.mdpi.com/2072-4292/13/11/2196 doi: 10.3390/rs13112196

Frenken, K. (2005). *Irrigation in Africa in figures: AQUASTAT survey, 2005* (K. Frenken & F. a. A. O. of the United Nations, Eds.) (No. 29). Rome: Food and Agriculture Organization of the United Nations. (OCLC: ocm64664575)

Gal, L., Grippa, M., Hiernaux, P., Peugeot, C., Mougin, E., & Kergoat, L. (2016). Changes in lakes water volume and runoff over ungauged sahelian watersheds. *Journal of Hydrology*, *540*, 1176–1188. Retrieved 2023-08-18, from https://linkinghub.elsevier.com/retrieve/pii/S0022169416304656 doi: 10.1016/j.jhydrol.2016.07.035

Galle, S., Grippa, M., Peugeot, C., Moussa, I. B., Cappelaere, B., Demarty, J., ... Wilcox, C. (2018). Amma-catch, a critical zone observatory in west africa monitoring a region in transition. *Vadose Zone Journal*, *17*(1), 180062. Retrieved from https://acsess.onlinelibrary.wiley.com/doi/abs/10.2136/vzj2018.03.0062 doi: https://doi.org/10.2136/vzj2018.03.0062

Gao, H., Birkett, C., & Lettenmaier, D. P. (2012). Global monitoring of large reservoir storage from satellite remote sensing. *Water Resources Research*, *48*(9), 2012WR012063. Retrieved 2023-11-01, from https://agupubs.onlinelibrary.wiley.com/doi/10.1029/2012WR012063 doi: 10.1029/2012WR012063

Gardelle, J., Hiernaux, P., Kergoat, L., & Grippa, M. (2010). Less rain, more water in ponds: a remote sensing study of the dynamics of surface waters from 1950 to present in pastoral sahel (gourma region, mali). *Hydrol. Earth Syst. Sci.*.

Girod, L., Nuth, C., Kääb, A., McNabb, R., & Galland, O. (2017). MMASTER: Improved ASTER DEMs for elevation change monitoring. *Remote Sensing*, *9*(7), 704. Retrieved 2023-10-06, from https://www.mdpi.com/2072-4292/9/7/704 doi: 10.3390/rs9070704

Gleick, P. (1993). *Water and conflict: Fresh water resources and international security.*

Gorelick, N., Hancher, M., Dixon, M., Ilyushchenko, S., Thau, D., & Moore, R. (2017). Google Earth Engine: Planetary-scale geospatial analysis for everyone. *Remote Sensing of Environment*, *202*, 18–27. Retrieved 2024-02-14, from https://linkinghub.elsevier.com/retrieve/pii/S0034425717302900 doi: 10.1016/j.rse.2017.06.031

Grippa, M., Rouzies, C., Biancamaria, S., Blumstein, D., Cretaux, J.-F., Gal, L., ... Kergoat, L. (2019). Potential of SWOT for monitoring water volumes in sahelian ponds and lakes. *IEEE Journal of Selected Topics in Applied Earth Observations and Remote Sensing*, *12*(7), 2541–2549. Retrieved 2023-08-18, from https://ieeexplore.ieee.org/document/8684868/ doi: 10.1109/JSTARS.2019.2901434

Haas, E., Bartholomé, E., & Combal, B. (2009). Time series analysis of optical remote sensing data for the mapping of temporary surface water bodies in sub-Saharan western Africa. *Journal of Hydrology*, *370*(1-4), 52–63. Retrieved 2024-01-29, from https://linkinghub.elsevier.com/retrieve/pii/S0022169409001413 doi: 10.1016/j.jhydrol.2009.02.052

Hilton, J. (1985). A conceptual framework for predicting the occurrence of sediment focusing and sediment redistribution in small lakes. *Limnology and Oceanography*, *30*(6), 1131–1143. Retrieved 2024-02-16, from https://aslopubs.onlinelibrary.wiley.com/doi/10.4319/lo.1985.30.6.1131 doi: 10.4319/lo.1985.30.6.1131

Hugonnet, R., Brun, F., Berthier, E., Dehecq, A., Mannerfelt, E. S., Eckert, N., & Farinotti, D. (2022). Uncertainty analysis of digital elevation models by spatial inference from stable terrain. *IEEE Journal of Selected Topics in Applied Earth Observations and Remote Sensing*, *15*, 6456–6472. Retrieved 2023-04-21, from https://ieeexplore.ieee.org/document/9815885/ doi: 10.1109/JSTARS.2022.3188922

Jasinski, M., Stoll, J., Hancock, D., Robbins, J., Nattala, J., Morison, J., ... Carabajal, C. (2023). Icesat-2 algorithm theoretical basis document (atbd)

for along track inland surface water data, atl13, version 6. *ICESat-2 Project*. doi: 10.5067/03JYGZ0758UL

Kannan, K. S., Manoj, K., & Arumugam, S. (2015). Labeling methods for identifying outliers. *International Journal of Statistics and Systems*, *10*(2), 231-238.

Kittel, C. M. M., Jiang, L., Tøttrup, C., & Bauer-Gottwein, P. (2021). Sentinel-3 radar altimetry for river monitoring – a catchment-scale evaluation of satellite water surface elevation from sentinel-3a and sentinel-3b. *Hydrology and Earth System Sciences*, *25*(1), 333–357. Retrieved 2023-06-23, from https://hess.copernicus.org/articles/25/333/2021/ doi: 10.5194/hess-25-333-2021

Kittler, J., & Illingworth, J. (1986). Minimum error thresholding. *Pattern Recognition*, *19*(1), 41–47. Retrieved 2022-06-13, from https://linkinghub.elsevier.com/retrieve/pii/0031320386900300 doi: 10.1016/0031-3203(86)90030-0

Li, Y., Gao, H., Zhao, G., & Tseng, K.-H. (2020). A high-resolution bathymetry dataset for global reservoirs using multi-source satellite imagery and altimetry. *Remote Sensing of Environment*, *244*, 111831. Retrieved 2022-09-09, from https://linkinghub.elsevier.com/retrieve/pii/S0034425720302017 doi: 10.1016/j.rse.2020.111831

Liebe, J., van de Giesen, N., & Andreini, M. (2005). Estimation of small reservoir storage capacities in a semi-arid environment. *Physics and Chemistry of the Earth, Parts A/B/C*, *30*(6-7), 448–454. Retrieved 2023-01-20, from https://linkinghub.elsevier.com/retrieve/pii/S1474706505000409 doi: 10.1016/j.pce.2005.06.011

Liu, A., Cheng, X., & Chen, Z. (2021). Performance evaluation of GEDI and ICESat-2 laser altimeter data for terrain and canopy height retrievals. *Remote Sensing of Environment*, *264*, 112571. Retrieved 2022-09-30, from https://linkinghub.elsevier.com/retrieve/pii/S0034425721002911 doi: 10.1016/j.rse.2021.112571

Lorensen, W. E., & Cline, H. E. (1987). Marching cubes: A high resolution 3d surface construction algorithm. *Computer Graphics*, 7.

Luo, S., Song, C., Ke, L., Zhan, P., Fan, C., Liu, K., ... Zhu, J. (2022). Satellite laser altimetry reveals a net water mass gain in global lakes with spatial heterogeneity in the early 21st century. *Geophysical Research Letters*, *49*(3). Retrieved 2023-06-22, from https://onlinelibrary.wiley.com/doi/10.1029/2021GL096676 doi: 10.1029/2021GL096676

Ma, Y., Xu, N., Sun, J., Wang, X. H., Yang, F., & Li, S. (2019). Estimating water levels and volumes of lakes dated back to the 1980s using Landsat imagery and photon-counting lidar datasets. *Remote Sensing of Environment*, *232*, 111287. Retrieved 2024-02-05, from https://linkinghub.elsevier.com/retrieve/pii/S0034425719303062 doi: 10.1016/j.rse.2019.111287

Magome, J., Ishidaira, H., & Takeuchi, K. (2003). Method for satellite monitoring of water storage in reservoirs for efficient regional water management. *IAHS-AISH publication*, 303-310. Retrieved from https://api.semanticscholar.org/CorpusID:132761153

Mahe, G., Diello, P., Paturel, J.-E., Barbier, B., Karambiri, H., Dezetter, A., ... Rouche, N. (2010). Baisse des pluies et augmentation des écoulements au Sahel: impact climatique et anthropique sur les écoulements du Nakambe au Burkina Faso. *Sécheresse*, *21*(4), 330–332. Retrieved 2023-09-02, from http://www.john-libbey-eurotext.fr/medline.md?doi=10.1684/sec.2010.0268 doi: 10.1684/sec.2010.0268

Markus, T., Neumann, T., Martino, A., Abdalati, W., Brunt, K., Csatho, B., ... Zwally, J. (2017). The ice, cloud, and land elevation satellite-2 (ICESat-2): Science requirements, concept, and implementation. *Remote Sensing of Environment*, *190*, 260–273. Retrieved 2023-10-30, from

https://linkinghub.elsevier.com/retrieve/pii/S0034425716305089 doi: 10.1016/j.rse.2016.12.029

Mason, D. C., Davenport, I. J., Robinson, G. J., Flather, R. A., & McCartney, B. S. (1995-12-01). Construction of an inter-tidal digital elevation model by the 'water-line' method. *Geophysical Research Letters*, *22*(23), 3187–3190. Retrieved 2023-07-25, from http://doi.wiley.com/10.1029/95GL03168 doi: 10.1029/95GL03168

Neuenschwander, A. L., Pitts, K. L., Jelley, B. P., Robbins, J., Markel, J., Popescu, S. C., ... Sheridan., R. (2023). *Atlas/icesat-2 l3a land and vegetation height, version 6.* NASA National Snow and Ice Data Center Distributed Active Archive Center. Retrieved from https://nsidc.org/data/ATL08/versions/6 doi: 10.5067/ATLAS/ATL08.006

Nicholson, S. E. (2018). Climate of the Sahel and West Africa. In *Oxford Research Encyclopedia of Climate Science.* Oxford University Press. Retrieved 2024-02-20, from http://climatescience.oxfordre.com/view/10.1093/acrefore/9780190228620.001.0001/acrefore-9780190228620-e-510 doi: 10.1093/acrefore/9780190228620.013.510

Normandin, C., Frappart, F., Diepkilé, A. T., Marieu, V., Mougin, E., Blarel, F., ... Ba, A. (2018). Evolution of the Performances of Radar Altimetry Missions from ERS-2 to Sentinel-3A over the Inner Niger Delta. *Remote Sensing*, *10*(6), 833. Retrieved 2023-07-13, from http://www.mdpi.com/2072-4292/10/6/833 doi: 10.3390/rs10060833

Nuth, C., & Kääb, A. (2011). Co-registration and bias corrections of satellite elevation data sets for quantifying glacier thickness change. *The Cryosphere*, *5*(1), 271–290. Retrieved 2023-03-10, from https://tc.copernicus.org/articles/5/271/2011/ doi: 10.5194/tc-5-271-2011

Oki, T., & Kanae, S. (2006). Global hydrological cycles and world water resources. *Science*, *313*(5790), 1068–1072. Retrieved 2024-01-02, from https://www.science.org/doi/10.1126/science.1128845 doi: 10.1126/science.1128845

Otsu, N. (1979). A threshold selection method from gray-level histograms. *IEEE Transactions on Systems, Man, and Cybernetics*, *9*(1), 62–66. Retrieved 2023-05-10, from http://ieeexplore.ieee.org/document/4310076/ doi: 10.1109/TSMC.1979.4310076

Pan, F., Liao, J., Li, X., & Guo, H. (2013). Application of the inundation area—lake level rating curves constructed from the SRTM DEM to retrieving lake levels from satellite measured inundation areas. *Computers & Geosciences*, *52*, 168–176. Retrieved 2023-10-12, from https://linkinghub.elsevier.com/retrieve/pii/S0098300412003342

Papa, F., Crétaux, J.-F., Grippa, M., Robert, E., Trigg, M., Tshimanga, R. M., ... Calmant, S. (2023). Water Resources in Africa under Global Change: Monitoring Surface Waters from Space. *Surveys in Geophysics*, *44*(1), 43–93. Retrieved 2023-09-01, from https://link.springer.com/10.1007/s10712-022-09700-9 doi: 10.1007/s10712-022-09700-9

Pekel, J.-F., Cottam, A., Gorelick, N., & Belward, A. S. (2016). High-resolution mapping of global surface water and its long-term changes. *Nature*, *540*(7633), 418–422. Retrieved 2022-09-30, from http://www.nature.com/articles/nature20584 doi: 10.1038/nature20584

Pham-Duc, B., Sylvestre, F., Papa, F., Frappart, F., Bouchez, C., & Crétaux, J.-F. (2020). The Lake Chad hydrology under current climate change. *Scientific Reports*, *10*(1), 5498. Retrieved 2024-02-12, from https://www.nature.com/articles/s41598-020-62417-w doi: 10.1038/s41598-020-62417-w

Pi, X., Luo, Q., Feng, L., Xu, Y., Tang, J., Liang, X., ... Bryan, B. A. (2022). Mapping global lake dynamics reveals the emerging roles of small lakes. *Nature Communications*, *13*(1), 5777. Retrieved 2024-01-02, from

https://www.nature.com/articles/s41467-022-33239-3 doi: 10.1038/s41467-022-33239-3

Ragettli, S., Donauer, T., Molnar, P., Delnoije, R., & Siegfried, T. (2021). *Unraveling the hydrology and sediment balance of an ungauged lake in the Sudano-Sahelian region of West Africa using remote sensing* (preprint). Cross-cutting themes: Digital Landscapes: Insights into geomorphological processes from high-resolution topography and quantitative interrogation of topographic data. Retrieved 2022-05-30, from https://esurf.copernicus.org/preprints/esurf-2021-99/ doi: 10.5194/esurf-2021-99

Reis, L. G. d. M., Souza, W. d. O., Ribeiro Neto, A., Fragoso, C. R., Ruiz-Armenteros, A. M., Cabral, J. J. d. S. P., & Montenegro, S. M. G. L. (2021). Uncertainties Involved in the Use of Thresholds for the Detection of Water Bodies in Multitemporal Analysis from Landsat-8 and Sentinel-2 Images. *Sensors*, *21*(22), 7494. Retrieved 2022-08-29, from https://www.mdpi.com/1424-8220/21/22/7494 doi: 10.3390/s21227494

Reynaud, A., & Lanzanova, D. (2017). A global meta-analysis of the value of ecosystem services provided by lakes. *Ecological Economics*, *137*, 184–194. Retrieved 2024-01-02, from https://linkinghub.elsevier.com/retrieve/pii/S0921800916309168 doi: 10.1016/j.ecolecon.2017.03.001

Riggs, R. M., Allen, G. H., Wang, J., Pavelsky, T. M., Gleason, C. J., David, C. H., & Durand, M. (2023). Extending global river gauge records using satellite observations. *Environmental Research Letters*, *18*(6), 064027. Retrieved 2023-12-14, from https://iopscience.iop.org/article/10.1088/1748-9326/acd407 doi: 10.1088/1748-9326/acd407

Rupnik, E., Daakir, M., & Pierrot Deseilligny, M. (2017). MicMac – a free, open-source solution for photogrammetry. *Open Geospatial Data, Software and Standards*, *2*(1), 14. Retrieved 2022-09-30, from http://opengeospatialdata.springeropen.com/articles/10.1186/s40965-017-0027-2 doi: 10.1186/s40965-017-0027-2

Sanogo, I., & Dezetter, A. (1997). *Etudes hydro-météorologiques du bassin de la comoé et bilan hydrologique des retenues de toussiana, lobi et mous-sodougou.* Retrieved from https://horizon.documentation.ird.fr/exl-doc/pleins_textes/griseli/010011178.pdf

Schallenberg, M., de Winton, M. D., Verburg, P., Kelly, D. J., Hamill, K. D., & Hamilton, D. P. (2013). Ecosystem services of lakes. *ECOSYSTEM SERVICES OF LAKES*.

Schwatke, C., Dettmering, D., Bosch, W., & Seitz, F. (2015). DAHITI – an innovative approach for estimating water level time series over inland waters using multi-mission satellite altimetry. *Hydrology and Earth System Sciences*, *19*(10), 4345–4364. Retrieved 2023-12-07, from https://hess.copernicus.org/articles/19/4345/2015/ doi: 10.5194/hess-19-4345-2015

Schwatke, C., Dettmering, D., & Seitz, F. (2020). Volume variations of small inland water bodies from a combination of satellite altimetry and optical imagery. *Remote Sensing*, *12*(10), 1606. Retrieved 2023-08-09, from https://www.mdpi.com/2072-4292/12/10/1606 doi: 10.3390/rs12101606

Schwatke, C., Scherer, D., & Dettmering, D. (2019). Automated Extraction of Consistent Time-Variable Water Surfaces of Lakes and Reservoirs Based on Landsat and Sentinel-2. *Remote Sensing*, *11*(9), 1010. Retrieved 2024-02-05, from https://www.mdpi.com/2072-4292/11/9/1010 doi: 10.3390/rs11091010

Smith, L. C., & Pavelsky, T. M. (2009). Remote sensing of volumetric storage changes in lakes. *Earth Surface Processes and Landforms*, *34*(10), 1353–1358. Retrieved 2023-01-17, from https://onlinelibrary.wiley.com/doi/10.1002/esp.1822 doi: 10.1002/esp.1822

Song, C., Huang, B., & Ke, L. (2013). Modeling and analysis of lake water storage changes on the Tibetan Plateau using multi-mission satellite data. *Re-*

mote Sensing of Environment, *135*, 25–35. Retrieved 2023-03-23, from https://linkinghub.elsevier.com/retrieve/pii/S0034425713000928 doi: 10.1016/j.rse.2013.03.013

Taburet, N., Zawadzki, L., Vayre, M., Blumstein, D., Le Gac, S., Boy, F., ... Femenias, P. (2020). S3mpc: Improvement on inland water tracking and water level monitoring from the OLTC onboard sentinel-3 altimeters. *Remote Sensing*, *12*(18), 3055. Retrieved 2023-06-23, from https://www.mdpi.com/2072-4292/12/18/3055 doi: 10.3390/rs12183055

Terekhov, A., Makarenko, N., Pak, A., & Abayev, N. (2020). Using the digital elevation model (DEM) and coastlines for satellite monitoring of small reservoir filling. *Cogent Engineering*, *7*(1), 1853305. Retrieved 2023-10-12, from https://www.tandfonline.com/doi/full/10.1080/23311916.2020.1853305 doi: 10.1080/23311916.2020.1853305

Tian, X., & Shan, J. (2021). Comprehensive evaluation of the ICESat-2 ATL08 terrain product. *IEEE Transactions on Geoscience and Remote Sensing*, *59*(10), 8195–8209. Retrieved 2022-09-30, from https://ieeexplore.ieee.org/document/9334397/ doi: 10.1109/TGRS.2021.3051086

Touré, A. A., Tidjani, A., Guillon, R., Rajot, J. L., Petit, C., Garba, Z., & Sebag, D. (2016). Teneur en matières en suspension des lacs sahéliens en liaison avec les variations piézométrique et pluviométrique: cas des lacs bangou kirey et bangou bi, sud-ouest niger. *Afrique SCIENCE*.

Tseng, K.-H., Shum, C. K., Kim, J.-W., Wang, X., Zhu, K., & Cheng, X. (2016). Integrating Landsat Imageries and Digital Elevation Models to Infer Water Level Change in Hoover Dam. *IEEE Journal of Selected Topics in Applied Earth Observations and Remote Sensing*, *9*(4), 1696–1709. Retrieved 2023-10-12, from https://ieeexplore.ieee.org/document/7383227/ doi: 10.1109/JSTARS.2015.2500599

Tully, K., Sullivan, C., Weil, R., & Sanchez, P. (2015). The State of Soil Degradation in Sub-Saharan Africa: Baselines, Trajectories, and Solutions. *Sustainability*, *7*(6), 6523–6552. Retrieved 2024-02-16, from http://www.mdpi.com/2071-1050/7/6/6523 doi: 10.3390/su7066523

Urbazaev, M., Hess, L. L., Hancock, S., Sato, L. Y., Ometto, J. P., Thiel, C., ... Schmullius, C. (2022). Assessment of terrain elevation estimates from ICESat-2 and GEDI spaceborne LiDAR missions across different land cover and forest types. *Science of Remote Sensing*, *6*, 100067. Retrieved 2023-10-05, from https://linkinghub.elsevier.com/retrieve/pii/S2666017222000293 doi: 10.1016/j.srs.2022.100067

Wang, J., Song, C., Reager, J. T., Yao, F., Famiglietti, J. S., Sheng, Y., ... Wada, Y. (2018). Recent global decline in endorheic basin water storages. *Nature Geoscience*, *11*(12), 926–932. Retrieved 2023-06-22, from https://www.nature.com/articles/s41561-018-0265-7 doi: 10.1038/s41561-018-0265-7

Wurtsbaugh, W. A., Miller, C., Null, S. E., DeRose, R. J., Wilcock, P., Hahnenberger, M., ... Moore, J. (2017). Decline of the world's saline lakes. *Nature Geoscience*, *10*(11), 816–821. Retrieved 2024-01-06, from https://www.nature.com/articles/ngeo3052 doi: 10.1038/ngeo3052

Xu, H. (2006). Modification of normalised difference water index (NDWI) to enhance open water features in remotely sensed imagery. *International Journal of Remote Sensing*, *27*(14), 3025–3033. Retrieved 2022-09-30, from https://www.tandfonline.com/doi/full/10.1080/01431160600589179 doi: 10.1080/01431160600589179

Xu, N., Ma, Y., Zhang, W., Wang, X. H., Yang, F., & Su, D. (2020). Monitoring Annual Changes of Lake Water Levels and Volumes over 1984–2018 Using Landsat Imagery and ICESat-2 Data. *Remote Sensing*, *12*(23), 4004. Retrieved 2024-02-05, from https://www.mdpi.com/2072-4292/12/23/4004

doi: 10.3390/rs12234004

Yang, X., Zhao, S., Qin, X., Zhao, N., & Liang, L. (2017). Mapping of Urban Surface Water Bodies from Sentinel-2 MSI Imagery at 10 m Resolution via NDWI-Based Image Sharpening. *Remote Sensing*, *9*(6), 596. Retrieved 2022-09-30, from http://www.mdpi.com/2072-4292/9/6/596 doi: 10.3390/rs9060596

Yao, F., Livneh, B., Rajagopalan, B., Wang, J., Crétaux, J.-F., Wada, Y., & Berge-Nguyen, M. (2023). Satellites reveal widespread decline in global lake water storage. *Science*, *380*(6646), 743–749. Retrieved 2023-05-24, from https://www.science.org/doi/10.1126/science.abo2812 doi: 10.1126/science.abo2812

Yao, F., Wang, J., Wang, C., & Crétaux, J.-F. (2019). Constructing long-term high-frequency time series of global lake and reservoir areas using Landsat imagery. *Remote Sensing of Environment*, *232*, 111210. Retrieved 2022-05-30, from https://linkinghub.elsevier.com/retrieve/pii/S0034425719302238 doi: 10.1016/j.rse.2019.111210

Yao, F., Wang, J., Yang, K., Wang, C., Walter, B. A., & Crétaux, J.-F. (2018). Lake storage variation on the endorheic tibetan plateau and its attribution to climate change since the new millennium. *Environmental Research Letters*, *13*(6), 064011. Retrieved 2023-06-07, from https://iopscience.iop.org/article/10.1088/1748-9326/aab5d3 doi: 10.1088/1748-9326/aab5d3

Zhang, S., & Gao, H. (2020). Using the digital elevation model (DEM) to improve the spatial coverage of the MODIS based reservoir monitoring network in south asia. *Remote Sensing*, *12*(5), 745. Retrieved 2023-11-01, from https://www.mdpi.com/2072-4292/12/5/745 doi: 10.3390/rs12050745

Zhang, Z., Bo, Y., Jin, S., Chen, G., & Dong, Z. (2023). Dynamic water level changes in qinghai lake from integrating refined ICESat-2 and GEDI altimetry data (2018–2021). *Journal of Hydrology*, *617*, 129007. Retrieved 2023-12-08, from https://linkinghub.elsevier.com/retrieve/pii/S0022169422015773 doi: 10.1016/j.jhydrol.2022.129007

Zolá, R. P., & Bengtsson, L. (2007). Three methods for determining the area–depth relationship of Lake Poopó, a large shallow lake in Bolivia. *Lakes & Reservoirs: Science, Policy and Management for Sustainable Use*, *12*(4), 275–284. Retrieved 2022-07-07, from https://onlinelibrary.wiley.com/doi/10.1111/j.1440-1770.2007.00344.x doi: 10.1111/j.1440-1770.2007.00344.x